# Atmospheric implications of increased Hydrogen use

Nicola Warwick, Paul Griffiths, James Keeble, Alexander Archibald, John Pyle, University of Cambridge and NCAS
and Keith Shine, University of Reading

April 2022

**Acknowledgements**

We thank Fiona O'Connor, Met Office, for assistance with the ERF analysis.

This work used Monsoon2, a collaborative High Performance Computing facility funded by the Met Office and the Natural Environment Research Council, JASMIN, the UK collaborative data analysis facility, and the NEXCS High Performance Computing facility funded by the Natural Environment Research Council and delivered by the Met Office.

© Crown copyright 2022

This publication is licensed under the terms of the Open Government Licence v3.0 except where otherwise stated. To view this licence, visit nationalarchives.gov.uk/doc/open-government-licence/version/3 or write to the Information Policy Team, The National Archives, Kew, London TW9 4DU, or email: psi@nationalarchives.gsi.gov.uk.

Where we have identified any third-party copyright information you will need to obtain permission from the copyright holders concerned.

Any enquiries regarding this publication should be sent to us at:
enquiries@beis.gov.uk

# Contents

`Atmospheric implications of increased hydrogen use

Abbreviations

AGWP Absolute Global Warming Potential

AR6 the 6th Assessment Report of the Intergovernmental Panel on Climate Change https://www.ipcc.ch/assessment-report/ar6/

$BrO_x$ bromine oxides

CCS Carbon dioxide capture and storage

CFC chlorofluorocarbon; specific compounds are identified by a number

$CH_4$ methane

$ClO_x$ chlorine oxides

CMIP6 6th phase of the Coupled Model Intercomparison Project

CDNC cloud droplet number concentration

CO carbon monoxide

$CO_2$ carbon dioxide

DU Dobson Unit

GMST global mean surface temperature

GWP global warming potential, relative to carbon dioxide

GWP(x) global warming potential relative to carbon dioxide over x years

$H_2$ Hydrogen

$H_2O$ water

$HO_2$ hydroperoxyl radical

$HO_x$ hydrogen oxides

$h\nu$ photon

IPPC Intergovernmental Panel on Climate Change

LBC lower boundary layer of the atmosphere

NOx oxides of nitrogen

$NO_2$ nitrogen dioxide

ppb parts per billion ($10^{-9}$)

ppm parts per million ($10^{-6}$)

O ($^1D$) oxygen atoms in an electronically excited state

$O_2$ Oxygen

$O_3$ Ozone

OH hydroxyl radical

R a hydrocarbon part of a molecule

SMR steam methane reformation

SSP Shared socioeconomic pathway

Tg teragram $10^{12}$ grammes equivalent to a megaton

UKCA UK Chemistry and Aerosols model (http://www.ukca.ac.uk/)

UKESM  UK Earth System Model (https://ukesm.ac.uk/)

UNFCCC United Nations Framework Convention on Climate Change

US EPA United States Environmental Protection Agency

VOCs volatile organic compounds

# Executive Summary

Use of hydrogen ($H_2$) as a substitute for carbon-containing fossil fuels such as natural gas would prevent emissions of carbon dioxide into the atmosphere, with significant climate benefits. Nevertheless, any leakage of hydrogen will affect atmospheric composition (with implications for air quality) and have an indirect warming effect on climate, partially offsetting some of the climate benefits of the reduction in carbon dioxide.

We have explored the possible impact of hydrogen leakage using a chemistry/climate model of the atmosphere. Uncertainties in hydrogen leakage rates, the extent to which hydrogen might replace fossil fuels in the future and future hydrogen uptake rates by soils, make it difficult to predict accurately changes to atmospheric hydrogen mixing ratios in a hydrogen economy. We have considered a range of possible hydrogen future global scenarios, with surface mixing ratio increases ranging from 0.25 parts per million (50% increase) by volume (ppm or millimoles/mole) to 1.5 ppm (300% increase) above the current background mixing ratio of about 0.5 ppm. We believe these scenarios span much of the uncertainty in potential changes to the atmospheric mixing ratios of hydrogen associated with the ultimate size of the hydrogen economy, the hydrogen soil sink and hydrogen leakage rates. For example, a 1.5 ppm increase in the surface hydrogen mixing ratio would be consistent with a high leakage rate of 20% in a global hydrogen economy providing 23% of present day global energy consumption, where the magnitude of the soil sink of hydrogen increases linearly with hydrogen mixing ratios; it would also be consistent, for the same energy consumption, with a constant magnitude, fixed soil sink and an hydrogen leakage rate of about 4%. Use of this range of global scenarios provides a clear signal in the atmospheric response to increased hydrogen mixing ratios relative to interannual variability and also allows us to explore the linearity of the atmospheric response to increasing hydrogen. We have also considered the impact of changes in emissions of gases other than carbon dioxide ($CO_2$) which could follow increased adoption of Hydrogen as an energy source; these gases, emitted alongside carbon dioxide and called hereafter ‘co-emitted species’, include carbon monoxide (CO), methane ($CH_4$), volatile organic compounds (VOCs) and the oxides of nitrogen (NOx).

## Atmospheric Composition

**Leakage of hydrogen into the atmosphere will decrease the tropospheric concentration of hydroxyl radicals (OH), the major tropospheric oxidant, and thereby increase the atmospheric lifetime of methane and its impact on climate.**

The change in hydroxyl radicals is linear in the hydrogen increase when other emissions are constant; for every 1 ppm increase in hydrogen, tropospheric mean hydroxyl radical concentration decreases by about $0.90 \times 10^5$ molecule $cm^{-3}$.

Similarly, the change in the methane lifetime is linear in hydrogen; the lifetime increases by about a year for every 1 ppm increase in hydrogen.

Calculations in which emissions of co-emitted species change also exhibit this linearity, but with different gradients.

**The future change in methane ($CH_4$) concentration in the atmosphere will depend both on the hydrogen-induced change in lifetime and the changes in methane emissions which would follow adoption of a hydrogen economy.**

Our box model calculations indicate that, under the influence of the hydroxyl radical change induced by a 1.5 ppm increase in hydrogen alone (the largest hydrogen increase considered here), the methane concentration will increase by about 340 ppb. Even if methane emissions are reduced the effect of hydrogen leakage on hydroxyl radical concentrations could still lead to a rise in methane concentrations.

**An increase in the atmospheric concentration of hydrogen, assuming no change in other emissions, will increase tropospheric ozone ($O_3$).**

The change in tropospheric ozone burden is linear in hydrogen  increase. A 1.5 ppm increase in hydrogen leads to a small, approximately 6.5 Tg (~1.8%) increase in the tropospheric ozone burden.

**Tropospheric ozone is important for both air quality and climate. How it changes in response to the adoption of a hydrogen economy will depend not just on the increase in hydrogen but also on the benefits arising from any associated reductions in the emissions of methane, carbon monoxide, volatile organic compounds and oxides of nitrogen, which will tend to decrease ozone concentrations.**

There is uncertainty in exactly how co-emissions will change both in magnitude and regionally as the scale of change will depend on hydrogen production methods and the technologies replaced by hydrogen. For example, in scenarios involving co-emitted species, we have assumed reductions in carbon monoxide, volatile organic compounds and oxides of nitrogen, although in sectors where hydrogen is burnt there could be increases in oxides of nitrogen emissions.

**There is no significant difference in the tropospheric ozone response to increasing hydrogen under present day and future (2050) climate states.**

The magnitude and spatial pattern of tropospheric ozone increases associated with an increase in atmospheric hydrogen mixing ratios is similar under both present day and future (2050) conditions, assuming future emissions follow the SSP2-4.5 climate scenario, representative of a middle of the road scenario of future society.

`Atmospheric implications of increased hydrogen use

**An increase in the atmospheric concentration of hydrogen leads to decreases in upper stratospheric ozone mixing ratios.**

As atmospheric hydrogen increases, upper stratospheric (>40 km altitude) ozone mixing ratios decrease. A 1.5 ppm increase in hydrogen leads to about a 5% decrease in ozone mixing ratios. For the largest hydrogen emissions considered in this study, polar lower stratospheric ozone mixing ratios also show statistically significant reductions.

**There is no discernible impact on annual mean, global mean total column ozone recovery of adoption of a global hydrogen economy.**

Total column ozone changes are dependent on both the stratospheric reductions and tropospheric increases in ozone mixing ratios described above. There is no statistically significant reduction in total column ozone values, averaged over 60ºS-60ºN, for a 1.5 ppm increase in hydrogen under either present day or 2050 conditions. However, Antarctic springtime total column ozone may see some increased depletion under very large hydrogen emissions, but this is dependent also on assumptions about changes to atmospheric methane.

**Hydrogen leakage will lead to increases in water vapour throughout the atmosphere, with potentially significant increases in the stratosphere.** The scenario with a 1.5 ppm increase in hydrogen shows a greater than 1 ppm increase in water (H2O) in the upper stratosphere.

# Radiative forcing

**Adoption of hydrogen as an energy source could reduce emissions of carbon dioxide and provide a significant climate benefit.** The benefit is maximised by reducing leakage of hydrogen and reducing the co-emissions of climate warming gases.

**Increases in tropospheric ozone, water vapour and methane, consequent on increases in atmospheric hydrogen, would all tend to increase radiative forcing, partially offsetting the climate benefits of a switch to hydrogen.**

**The net top-of-atmosphere radiative forcing will depend strongly on the hydrogen leakage rate, on any associated reduction in methane emissions and on the extent of co-emission benefits.**

When only hydrogen increases in our model experiments, we calculate an effective radiative forcing of 0.148 W $m^{-2}$ for an increase in hydrogen of 1.5 ppm; when the methane lower boundary is increased by 340 ppb, consistent with the decrease in hydroxyl radicals, the radiative forcing approaches 0.5 W $m^{-2}$ (a warming tendency). In contrast, if there is no leakage of hydrogen into the atmosphere, and methane and other co-emissions are reduced, the change in radiative forcing is -0.29 W $m^{-2}$ (a cooling tendency). Assuming an equilibrium climate sensitivity of 0.86 K $W^{-1}$ $m^2$, this level of radiative forcing if sustained would lead to global-mean temperature changes of 0.12, 0.43 and -0.26 ˚C (without accounting for the reduced emissions of carbon dioxide that would result).

`Atmospheric implications of increased hydrogen use

**The net top-of-atmosphere radiative forcing varies strongly regionally. It depends in a complex fashion on the changes in gas phase composition, the subsequent impact on aerosol production and on cloud and aerosol interactions.**

# Global warming potential of hydrogen

**We have developed a new approach to calculating Global Warming Potentials (GWPs) for species whose emissions result in indirect radiative forcings**. Unlike previous methods, our new approach considers the lifetime of the pulse gas in addition to the lifetimes of the radiatively active gases causing the indirect forcing. This allows GWPs arising from indirect forcings to be calculated for gases with intermediate and longer lifetimes, such as hydrogen.

**In addition to changes in methane and ozone in the troposphere, we have also considered previously ignored changes in stratospheric water vapour and stratospheric ozone in our calculations of hydrogen's GWP.**

**Our estimate of the hydrogen GWP for a 100 year time horizon is 11 ± 5, which is more than 100% larger than previously published calculations.** Approximately one third of the GWP arises due to the stratospheric response, which was not considered in previous studies. The majority of uncertainty in the GWP arises from uncertainty in the magnitude of the soil sink for hydrogen.

# Some policy implications

**Leakage of hydrogen into the atmosphere during production, storage, distribution and use will partially offset some of the benefits of a hydrogen-based economy. Minimisation of leaks needs to be a priority if hydrogen is adopted as a major energy source.**

**Use of hydrogen provides an opportunity to reduce emissions of species which might be co-emitted during the production of carbon dioxide. Reductions in emissions of methane, carbon monoxide, volatile organic compounds and oxides of nitrogen would all provide both climate and air quality benefits. Maximising these reductions should be a further policy priority.**

# Future work

**There remain uncertainties with regard to the natural budget of atmospheric hydrogen**. The hydrogen lifetime is dominated by its surface sink. The lack of detailed understanding of the sink is a major source of uncertainty in calculations of hydrogen change and its impact on climate.

`Atmospheric implications of increased hydrogen use

**Future model calculations should explore alternative ways to calculate the climate impact of hydrogen leakage into the atmosphere**. Complementary transient experiments, driven by fluxes of hydrogen and methane at the lower boundary, should be performed.

# 1 Introduction

Adoption of low carbon hydrogen ($H_2$) as an energy source should lead to substantial reductions in carbon emissions and a significant climate benefit. However, leakage of $H_2$ into the atmosphere during its production, storage, distribution and use could somewhat reduce the climate benefit and also have implications for air quality. This report focusses on the potential impacts of an increase in the abundance of atmospheric $H_2$.

$H_2$ is currently present in the atmosphere with a mixing ratio of about 0.55 parts per million (ppm). Present day sources of $H_2$ include fossil fuel combustion and biomass burning which are estimated to represent approximately 50% of the total global $H_2$ source, with the remainder arising from the oxidation of methane ($CH_4$) and volatile organic compounds (VOCs) in the atmosphere (e.g. Ehhalt and Rohrer 2009; Pieterse et al., 2013). Atmospheric $H_2$ is removed primarily by uptake to soils, but also through reaction with hydroxy radicals (OH) in the atmosphere. OH is the main oxidant that reacts with a range of species, hence altering its concentration could induce chemical feedbacks if $H_2$ emissions were to increase. Whilst current global levels of $H_2$ are relatively well constrained by atmospheric observations, the relative contributions of individual sources and sinks of $H_2$ are less well defined. In particular, there are large uncertainties associated with the size of the $H_2$ soil sink, due to limited understanding of the processes involved and large challenges associated with the geographical extrapolation of local measurements of $H_2$ uptake.

The principal chemical fate of $H_2$ is reaction with OH:

$H_2 + OH = H_2O + H$ (R1)

This reaction is an important sink for OH. It reduces OH and leads to an increase in $HO_2$, following the recombination of H with $O_2$. OH is a key tropospheric constituent. It is the major oxidant in the troposphere and plays a vital role in the budget of tropospheric ozone.

An important consequence of any increase in atmospheric $H_2$, and the subsequent decrease in OH, would be to increase the lifetime of $CH_4$, which is largely controlled by the reaction with OH

$CH_4 + OH = CH_3 + H_2O$ (R2)

Methane is second only to $CO_2$ in its impact as an anthropogenic greenhouse gas; lengthening the lifetime of $CH_4$ increases its radiative forcing (for a given $CH_4$ emission) and global warming potential. So, emissions of $H_2$ into the atmosphere would contribute indirectly to radiative forcing; $H_2$ is an indirect greenhouse gas.

Ozone ($O_3$) is another greenhouse gas. It is also a key air quality gas where high surface concentrations can be damaging to human health and surface vegetation.

`Atmospheric implications of increased hydrogen use

Ozone is produced in the troposphere by a complex series of reactions involving $NO_x$ and CO, $CH_4$ and volatile organic compounds (VOCs). The rate controlling reaction in ozone producing mechanisms is that between NO and peroxy radicals

$NO + RO_2 = NO_2 + RO$ (R3)

followed by photolysis of $NO_2$ to form ozone

$NO_2 + h\nu = NO + O$ ( $+O_2 = O_3$) (R4)

$HO_2$ is the most important peroxy radical but many organic radicals, the breakdown products of $CH_4$ and a range of VOCs, play some role. An increase in $H_2$ will lead, via reaction R1, to an increase in $HO_2$ and, in a $NO_x$-rich environment, to an increase in tropospheric ozone. Of course, use of $H_2$ as a fuel should not only decrease emissions of carbon dioxide but also lead to decreases in the emissions of $NO_x$, CO and VOCs (although $NO_x$ emissions could increase in some sectors); these reductions will tend to decrease tropospheric ozone production. Similarly, the future tendency of $CH_4$ depends not just on how OH changes but also on its direct emissions; a reduction in atmospheric $CH_4$ will tend to reduce tropospheric ozone.

Changes in $H_2$ will also affect atmospheric water vapour. The $H_2O$ abundance in the troposphere is dominated by the hydrological cycle but increases in atmospheric $H_2$ will likely lead to an increase in stratospheric water vapour. The radiative impacts of stratospheric water vapour are important and so deserve attention in the context of the indirect climate impact of $H_2$. Furthermore, increases in $H_2$ and $H_2O$ in the stratosphere will lead to the production of hydrogen radicals, which are involved in ozone destruction cycles. The Montreal Protocol is leading to the recovery of the stratospheric ozone layer. The extent to which future changes in $H_2$ might affect the recovery also needs to be investigated.

These different chemical and radiative effects have been studied here using numerical models of the atmosphere. A chemistry-climate model, UKESM1, in which the level of $CO_2$ is specified, is used to calculate the change in the global distribution of the other key climate and air quality species mentioned above under a range of different conditions and assumptions. UKESM1 employs fixed surface lower boundary concentrations for both $H_2$ and $CH_4$. Complementary integrations using a box model are used to define the boundary conditions employed in UKESM1 for these two gases. The models are described in Section 2. Section 3 discusses a number of potential hydrogen economy scenarios, including possible changes in the emissions of $H_2$, $CH_4$ and co-emitted species including CO, $NO_x$ and some VOCs. Based on this discussion a series of model integrations are defined covering conditions for the present day and the year 2050. These integrations explore (i) the impact of changes in the $H_2$ lower boundary condition alone, (ii) the impact of changes in $H_2$ and anthropogenic ozone precursors (CO, VOCs, etc), (iii) the impact of $CH_4$ changes consequent on the changes in $H_2$, (iv) the combined impact of changes in $CH_4$ and other anthropogenic ozone precursors. The composition changes which follow from the various integrations are presented in Section 4 while consequent changes in effective radiative forcing are given in Section 5. Section 6 presents a new calculation of the Global Warming Potential for $H_2$ and associated uncertainties.

# 2 The Models

For this work, as mentioned above, we adopt a complementary modelling strategy using both reduced-complexity 'box' models, in which the atmospheric mixing is presumed instantaneous, and more complex, and expensive, three-dimensional models to quantify transport and mixing effects. The models are described next.

## 2.1 The UKESM1 Earth system model

As part of this work, 18 timeslice simulations have been performed with the UKESM1 model. The UKESM1 model (Sellar et al., 2020) is a fully coupled Earth system model developed jointly by the United Kingdom's Met Office and Natural Environment Research Council. To isolate the effects of $H_2$ changes on atmospheric chemistry and climate we have utilised the atmosphere only version of UKESM1, switching off feedbacks from the ocean and land surface, following the AerChemMIP protocol (Collins et al., 2017). The model uses the UK Chemistry and Aerosols (UKCA) atmospheric chemistry module (Archibald et al., 2020) to simulate atmospheric composition. UKCA includes detailed representation of both tropospheric and stratospheric chemical processes, and couples chemical, radiative and dynamical processes from the surface to the top of the model (85 km), enabling a holistic treatment of ozone ($O_3$), the third most important radiatively active gas in the atmosphere and the primary source of the hydroxyl radical (OH) in the troposphere. In total, the chemistry solves 291 thermal and photolytic reactions which describe the chemistry of 81 species. This includes the oxidation reactions which are a source of sulphate and secondary organic aerosol, and hence the chemistry is tightly coupled to aerosol production. In our integrations here, $CO_2$ is held constant at values appropriate to present day or 2050 and plays no role in the chemistry scheme.

UKCA influences the model radiation scheme through the three-dimensional concentrations of four gases: $O_3$, $CH_4$, nitrous oxide ($N_2O$), and $H_2O$. UKCA $O_3$ is fully interactive and responds to surface emissions of ozone precursors such as VOCs, three-dimensional emissions of $NO_x$ (including emissions from aircraft and interactive production by lightning), concentrations of ozone depleting substances, and to changes in modelled climate associated with the hydrogen economy scenarios explored in this work. Chemical reactions which produce or destroy water vapour are modelled within UKCA and alter the humidity tracer of the dynamical core, allowing interactive simulation of chemical water vapour feedbacks.

In contrast to $O_3$, $CH_4$, $H_2$ and $N_2O$ are forced with prescribed globally constant mixing ratios at the surface (referred to as a lower boundary condition, or LBC), and above the surface are treated as interactive chemical tracers. This allows the model to represent the spatial variability of these species (in particular their decay in the upper troposphere and stratosphere) while broadly constraining their global concentrations to match the particular scenarios used for the simulation. In this work, changes to the $CH_4$ surface concentrations (either as a change to $CH_4$ emissions or as a response to changes in OH concentrations) are calculated using a box

model (see Section 2.2). This allows for the separation of the $CH_4$ response from the rest of the atmospheric composition changes induced by a shift to different hydrogen economy scenarios.

$H_2$ is modelled within UKCA in the same way as $CH_4$: $H_2$ mixing ratios follow a prescribed LBC at the surface, while above the surface $H_2$ is treated as an interactive chemical tracer. $H_2$ is not included in the model radiation scheme but does have an indirect radiative impact through chemical coupling with $O_3$, $CH_4$ and $H_2O$, and changes to these species are important when estimating the global warming potential of $H_2$ (see Section 6).

As a chemically inert gas, $CO_2$ is not modified by UKCA chemistry and is specified as a global constant in UKESM1. For the simulations explored here $CO_2$ is specified with the 2014 surface mixing ratio (397.6 ppm) for the TS2014 experiments, and the 2050 surface mixing ratio (506.9 ppm) taken from the SSP2-4.5 scenario for the TS2050 simulations. Changes to atmospheric $CO_2$ mixing ratios associated with a shift to a global hydrogen economy are not considered in the scenarios explored in this work; however expected changes in $CO_2$ emissions are discussed further in relation to the GWP determined for $H_2$ in Section 6.4.

## 2.2 Atmospheric composition box model

Box models, which are zero-dimensional models designed to simulate whole-atmosphere mixing ratios, are well-suited to the treatment of species whose atmospheric lifetime is long compared to the inter-hemispheric mixing time and which become well-mixed throughout the troposphere. In the case of $CH_4$ (lifetime approx. 9.6 ± 1.3 years, Prather et al., 2012) and $H_2$ (with a tropospheric lifetime of around 2 years, see Ehhalt and Rohrer, 2009; Section 6.3) this is a valid approach given a typical inter-hemispheric mixing time of around 1 year (as derived from $SF_6$ measurements, e.g. Yang et al., 2019). Our box modelling approach is similar to that described in Prather (1994) and used by the authors of this report in other studies (Heimann et al., 2020; Nisbet et al., 2020).

The mixing ratio of key species, $CH_4$, $H_2$ and CO are controlled by reaction with tropospheric OH and we summarise the chemical scheme below, in which [X] represents the concentration of species X, $S_x$ its source strength, $k_1$, $k_2$ and $k_3$ the relevant reaction rate constants and $\tau_{dep}$ is the lifetime of $H_2$ with respect to soil deposition. These kinetic equations describing the time evolution and final levels were calculated using a 4th order Runge Kutta numerical scheme using adaptive time stepping and validated by analysis of the system of equations using standard linear algebra techniques to verify the time constants for this coupled system.

$$\frac{d[CH_4]}{dt} = S_{CH4} - k_1[OH][CH_4]$$

$$\frac{d[H_2]}{dt} = S_{H2} - k_2[OH][H_2] - \frac{1}{\tau_{dep}}[H_2]$$

$$\frac{d[CO]}{dt} = S_{CO} - k_3[OH][CO] + k_1[OH][CH_4]$$

`Atmospheric implications of increased hydrogen use

$$\frac{d[OH]}{dt} = S_{OH} - k_X[OH] - k_3[OH][CO] - k_2[OH][H_2] - k_1[OH][CH_4]$$

While the reaction of $H_2$ with OH is an important $H_2$ sink, the largest sink is deposition to the surface, which also represents a key source of uncertainty for the future evolution of $H_2$ and its impact on climate (see Section 6.3).

The equations above show strong coupling between $CH_4$, $H_2$ and OH, mediated by oxidation of $CH_4$ to CO which functions as an additional OH sink. This non-linearity gives rise to $CH_4$self-feedback, in which an increase in $CH_4$ emissions generates an additional suppression of the OH sink, enhancing the $CH_4$ concentrations over that expected from the emissions increase itself.

The model was initialised with realistic values for total $CH_4$ emissions (585 Tg($CH_4$) per year), CO (1300 Tg(CO) per year) and $H_2$ (80 Tg($H_2$) per year) (e.g. Saunois et al., 2020; Pieterse et al., 2013; Zheng et al., 2019), and was found to give $CH_4$ and $H_2$ levels in broad agreement with present day levels – 1865 parts per billion (ppb) $CH_4$, 552 ppb $H_2$ and 101 ppb CO, as well as a $CH_4$ lifetime of 9.9 years, which is within the range of observationally-derived values.

We used the box model to obtain boundary condition values of $H_2$ and $CH_4$ for the three-dimensional chemistry-climate experiments and for extensive testing of the framework for GWP calculations. We employed the scenarios developed in Section 3 to simulate the effect of enhanced leakage of $H_2$ on atmospheric $H_2$ and on the coupled $CH_4$-$H_2$-OH system. The increase in $H_2$ levels results in lower levels of the OH oxidant and suppression of the $CH_4$ sink. Thus, $H_2$ emissions indirectly increase $CH_4$ levels. In the UKESM1 experiments for year 2014 and year 2050 conditions, we used the box model to calculate the enhanced/suppressed $CH_4$ levels caused by increases in $H_2$ emissions and decreased $NO_x$ emissions. 2014 was chosen as it represents the last year of the CMIP6 Historic global emissions datasets, and as such is observationally constrained (2015 onwards use the SSP-RCP emissions generated by IAMs and so are future projections). Details for the various scenarios are given below.

# 3 Hydrogen Economy Scenarios

To explore the potential impacts on atmospheric composition and radiative forcing of a global shift towards a hydrogen economy, a series of scenarios needs to be devised which include changes to the surface mixing ratio of $H_2$, associated reductions in other anthropogenic emissions as these sources are replaced with $H_2$ alternatives, and associated changes to atmospheric $CH_4$ in response to changes in $H_2$. Furthermore, these scenarios need to span a broad possible range of $H_2$ surface mixing ratios which cover different sizes of and/or leakage rates from the H2 infrastructure. We have chosen to consider a global hydrogen economy scenario rather than a UK-only focused scenario to ensure the atmospheric impacts are large enough to show a clear response to increased atmospheric $H_2$ levels in a global model. However by considering a range of $H_2$ surface mixing ratios we are able to assess the linearity of the response, allowing the atmospheric impact of smaller changes in $H_2$, such as might be induced by a UK-only switch to a hydrogen economy, to be determined. As the atmospheric lifetime of $H_2$ (at approximately 2 years) is longer than transport timescales in the lower atmosphere, H2 is relatively well-mixed and the exact region of $H_2$ emission (i.e. U.K. or global) is not anticipated to have a strong influence on the atmospheric response.

In this section we define the hydrogen economy scenarios considered in our UKESM1 simulations, along with the energy usage data, emission data and atmospheric box modelling that has been used to inform the changes to emissions and lower boundary conditions in each UKESM1 scenario. The background data that informs the scenarios is presented in Sections 3.1 to 3.3, and the final list of scenarios outlined in Section 3.4.

## 3.1 Hydrogen Leakage in a Hydrogen Economy

The change in $H_2$ emissions resulting from a hydrogen economy will depend on the level of $H_2$ usage in different energy sectors and the percentage of $H_2$ that leaks to the atmosphere during its production, transport and storage. Due to uncertainties in both $H_2$ leakage rates and the extent to which $H_2$ might replace fossil fuels in future, we perform a number of model simulations considering a range of different prescribed $H_2$ lower boundary concentrations to assess the impact of increases in $H_2$ on atmospheric composition. By considering a range of $H_2$ lower boundary conditions we are also able to investigate the linearity of the atmospheric response to increasing $H_2$.

To inform the range of $H_2$ lower boundary conditions to be considered, we estimate $H_2$ emissions from an illustrative future scenario where widespread use of $H_2$ has been adopted globally. In this scenario, we assume that set percentages of the final energy consumption in specified energy sectors, currently supplied by fossil fuel, switch to H2. We do not consider changes in emissions resulting from any other potential replacements for fossil fuel that may be used alongside $H_2$ (e.g. a move from petrol/diesel to electric cars). Uses for $H_2$ include heating in buildings, where $H_2$ could be blended into existing natural gas networks or used directly in $H_2$ boilers; transport, where other low carbon fuel options are limited; and power

generation, where $H_2$ could be used to store renewable energy and also used in gas turbines to increase power system flexibility. We have not considered the possible use of $H_2$ as an aviation fuel; production of water vapour from $H_2$ injected into the low stratosphere would have a radiative and chemical impact which has not been assessed here. In our illustrative scenario, 100% of the final energy consumption of fossil fuels in the buildings sector switches to $H_2$, along with 50% of the final energy consumption of fossil fuels in the transport sector and 10% of the final energy consumption of fossil fuels in the power generation sector. The lower percentages for transport and power generation reflect the smaller role $H_2$ is assumed to play in these energy sectors due to the existence of low carbon alternatives such as electric vehicles and wind and solar power together with alternative storage options such as pumped hydro, batteries and compressed air (e.g. Staffell et al., 2019). In total, this represents a scenario in which approximately 23% of global energy consumption (about 133 EJ) is supplied by $H_2$ (BP, Energy Outlook, 2020).

By combining the above assumptions on the proportions of each energy sector switching to $H_2$ with final global energy consumption data for 2018 from BP Energy Outlook (2020), together with information on the relative energy efficiencies of relevant fossil fuel and $H_2$ technologies, we estimate the $H_2$ needed to supply the required energy (Table 1). Our assumptions include (i) the energy efficiency of $H_2$ technologies in the buildings sector is the same as that for fossil fuels (based primarily on the assumption that $H_2$ boilers will operate at the same efficiency as those run on natural gas), (ii) diesel and petrol vehicles with an average tank-to-wheel energy efficiency of 30% will be replaced by vehicles using $H_2$ fuel cells with an average efficiency of 50%, (iii) electricity generated using $H_2$ has same energy efficiency as fossil fuel to electricity (Staffell et al. 2019). Using conversion factors of 1 tonne of oil equivalent (toe) = 11630 kWh and 1 kg $H_2$ = 33.3 kWh, we then estimate potential annual $H_2$ leakage rates by considering lower and upper leakage rates of 1% and 10%. $H_2$ leakage rates from the infrastructure associated with a hydrogen economy are uncertain and will depend on many factors (e.g. E4tech, 2019). However, all else being equal, $H_2$ leakage rates are likely to be higher than for natural gas owing to the small molecule size of $H_2$. A recent study looking at the US natural gas supply chain indicated natural gas leaks of around 2.3% of gross gas production, which is ~60% higher than the US EPA inventory estimate (Alvarez et al., 2018).

Based on an annual demand of 859 Tg $H_2$ to provide the required energy in the scenario outlined above (see Table 1), we estimate additional $H_2$ emissions due to $H_2$ leakage in a hydrogen economy to be 9 and 96 Tg $yr^{-1}$ based on leakage rates of 1 and 10% respectively. This change in $H_2$ emissions can be compared with the present day estimated total annual source of atmospheric $H_2$ of ~80 Tg $yr^{-1}$ (e.g. Pieterse et al., 2013). In our future 2050 simulations we assume a hydrogen economy of the same absolute magnitude, with identical $H_2$ leakage rates. However due to forecast changing energy demand over time, in the 2050 case the energy supplied by $H_2$ represents a different fraction of total energy consumption relative to our present day simulations.

Uncertainty in the global $H_2$ demand, due to both the extent that $H_2$ replaces fossil fuels and future changes to energy demand, will lead to further uncertainty in changes to $H_2$ emissions. However, it is clear that uncertainties in the leakage rate of $H_2$ currently have a significant impact on our ability to accurately predict changes in atmospheric $H_2$ in a hydrogen economy.

`Atmospheric implications of increased hydrogen use

When combined with the global widespread $H_2$-use described above, our upper leakage rate of 10% represents an upper limit on the increase in atmospheric $H_2$ associated with a hydrogen economy. A leakage rate of 10% would be likely to be both unsafe and expensive, leading to pressure for development of better containment.

Also significant for understanding future atmospheric $H_2$ mixing ratios in a hydrogen economy is the amount of $H_2$ currently emitted to the atmosphere from fossil fuel combustion. This is estimated to be ~20 Tg $yr^{-1}$, representing 20-25% of the total global $H_2$ source (e.g. Ehhalt and Rohrer, 2009; Pieterse et al., 2013). Any decreases in $H_2$ emissions resulting from a reduction in fossil fuel combustion may therefore partially offset any increases in $H_2$ emissions resulting from $H_2$ leakage in a hydrogen economy. This $H_2$ emission trade-off is not considered here, but should be considered as part of a study compiling a more detailed future hydrogen economy scenario.

**Table 1: Estimates of potential $H_2$ leakage in a global hydrogen economy.**

| | Final fossil fuel energy consumption (Million toe) | Percentage switch of final fossil fuel energy consumption to $H_2$ (%) | $H_2$ required to supply required energy consumption (Tg) | $H_2$ leakage at 1% (Tg $yr^{-1}$) | $H_2$ leakage at 10% (Tg $yr^{-1}$) |
|---|---|---|---|---|---|
| Buildings | 1298 | 100 | 453 | 4.6 | 50.4 |
| Transport | 2768 | 50 | 284 | 2.9 | 31.5 |
| Power | 3500 | 10 | 122 | 1.2 | 13.6 |
| Total | 7566 | 40 | 859 | 8.7 | 95.5 |

In UKESM1, $H_2$ is implemented using a prescribed constant mixing ratio at the surface. We use an atmospheric box model to relate the changes in $H_2$ emissions determined here with changes in the atmospheric $H_2$ mixing ratio required for our UKESM1 scenarios (see Section 3.3).

## 3.2 Emission reductions in methane, carbon monoxide, nitrogen oxides and volatile organic compounds

Surface emissions in our UKESM1 base scenario are described in Gidden et al. (2019), with a geographical emission distribution available for different energy sectors. A more detailed sector-by-sector breakdown for globally summed emissions is available in Hoesly et al. (2018). Emission reductions for $CH_4$, carbon monoxide (CO), $NO_x$ and volatile organic compounds (VOCs) in our illustrative hydrogen economy scenario (in which about 23% of global final

energy consumption is supplied by $H_2$) are determined by applying a uniform global scaling factor to emissions in the Gidden et al. (2019) energy sectors where $H_2$ is assumed to play a role. The emission reductions determined for $CH_4$ are converted to a change in the $CH_4$ lower boundary condition for UKESM1 using a box model (see Sections 2.2 and 3.3.2).

In our integrations, we assume that $H_2$ will be generated using a production method with no associated upstream $CH_4$ emissions (note $CO_2$ is fixed in our model simulations and changes to $CO_2$ emissions are therefore not considered). Today, the majority of $H_2$ is generated from steam methane reformation (SMR) which is associated with emissions of both $CH_4$ and carbon dioxide (unless $CO_2$ capture and storage is utilised). SMR has an energy efficiency of ~70%, therefore switching from natural gas to SMR $H_2$ would result in a greater quantity of $CH_4$ to supply the same level of final energy consumption, which could potentially lead to an increase in upstream $CH_4$ emissions. However, based on UNFCCC greenhouse gas inventory data (https://unfccc.int/process-and-meetings/transparency-and-reporting/greenhouse-gas-data/ghg-data-unfccc/ghg-data-from-unfccc ), the majority of $CH_4$ emissions in the UK arise from downstream leaks rather than during production (note that this was not the case for all Annex 1 countries). Using the UK UNFCC data for the ratio of upstream to downstream $CH_4$ emissions and assuming an energy efficiency for SMR of ~70% and that downstream $CH_4$ leaks are eliminated in an SMR scenario, we found only a minor impact on global $CH_4$ emissions between a green $H_2$ production scenario (i.e. zero associated upstream and downstream $CH_4$ emissions) and $H_2$ formed via steam methane reformation (SMR) including upstream methane emissions. A more detailed analysis accounting for the locations of $CH_4$ production sites and SMR locations, and the likely methane leakage during transport, would be required to accurately determine methane emissions in a hydrogen economy scenario using SMR. Other routes to low carbon hydrogen production are being proposed such as electrolysis or biomass gasification which may avoid upstream emissions of $CH_4$ and also $CO_2$ slip from the carbon capture and storage (CCS).

VOCs are represented in the UM-UKCA model by six tracers, lumped by species: ethane (lumped ethane, ethene and ethyne), propane (lumped propane and propene), formaldehyde, acetaldehyde (acetaldehyde lumped with other alkanals), acetone (acetone lumped with other ketones) and methanol. Many of these species have similar emission sources and we have therefore chosen to determine VOC emission reductions by applying single cross-species scaling factors for each energy sector.

### 3.2.1 Buildings Sector

In our hydrogen economy scenario, 100% of the energy supplied by fossil fuel in the buildings energy sector switches to $H_2$, and this is dominated by the switch to hydrogen boilers. To determine the associated emission reductions, we assume that the technology in the hydrogen boilers used is such that $NO_x$ emissions remain unaltered (despite the potential for higher $NO_x$ emissions from the increased flame temperature), whilst emissions of CO are eliminated. As buildings represent 92% of CO emissions in the Gidden ‘Residential, Commercial and Other’ sector (Hoesly et al. 2018), and assuming that fossil fuel accounts for 82% of CO emissions from fuel combustion in this sector (Galanter et al., 2000; Duncan et al., 2007), this leads to a 75% reduction in CO emissions in the ‘Residential, Commercial and Other’ energy sector.

`Atmospheric implications of increased hydrogen use

Switching from fossil fuel to $H_2$ in the buildings energy sector will also result in a reduction in $CH_4$ emissions in both the Gidden 'Residential, Commercial and Other' and 'Energy Production' sectors. In the Gidden 'Residential, Commercial and Other' sector, $CH_4$ emissions are decreased to zero. To determine the reduction in $CH_4$ emissions in the 'Energy Production' sector, we assume that buildings represent 21% of total natural gas consumption and 10% of total oil demand (BP, Energy Outlook, 2020), and fugitive emissions from gas and oil are reduced by these respective percentages. The contribution from coal is not available, but is assumed to be negligible in comparison to the uncertainty in these calculations. Based on UNFCCC greenhouse gas inventory data from Annex I countries (https://unfccc.int/process-and-meetings/transparency-and-reporting/greenhouse-gas-data/ghg-data-unfccc/ghg-data-from-unfccc), gas and oil represent 73% and 27% of combined fugitive oil and gas emissions respectively. This leads to a reduction in combined fugitive oil and gas emissions of 18%. From Hoesly et al. (2018), fugitive oil and gas emissions represent 58% of the 'Energy Production' sector emissions, leading to an overall reduction in $CH_4$ emissions from the Gidden 'Energy Production' sector of 10%.

VOC emissions from buildings are scaled according to calculated reductions in CO in the Gidden 'Residential, Commercial and Other' sector resulting in a 75% reduction, and $CH_4$ emissions in the Gidden 'Energy Production' sector resulting in a 10% reduction.

### 3.2.2 Transport Sector

In the transport sector, it is assumed that 50% of oil based transport is replaced by hydrogen fuel cells. Therefore, emissions of $CH_4$, CO, $NO_x$ and VOCs from the Gidden 'Transportation' energy sector are reduced by 50%. The associated reduction in global oil demand will also lead to a reduction in upstream $CH_4$ emissions in the Gidden 'Energy Production' sector. As transportation represents 57% of the global oil demand, replacing 50% of oil-based transport with $H_2$ results in a 28.5% reduction in fugitive oil $CH_4$ emissions. Based on UNFCCC greenhouse gas inventory data from Annex I countries (https://unfccc.int/process-and-meetings/transparency-and-reporting/greenhouse-gas-data/ghg-data-unfccc/ghg-data-from-unfccc), fugitive emissions from the oil sector contribute 27% of combined fugitive oil and gas $CH_4$ emissions, and from Hoesly et al. (2018), fugitive oil and gas emissions represent 58% of $CH_4$ emissions in the Gidden 'Energy Production' sector. This leads to an overall reduction in $CH_4$ emissions of 5% in the Gidden 'Energy Production' sector. A reduction of 5% is also applied to VOC emissions in the Gidden 'Energy Production' sector.

### 3.2.3 Power Sector

In our hydrogen economy scenario, stored $H_2$ will be used to generate 30% of the electricity currently generated using natural gas (in terms of the $H_2$ required, this is equivalent to 10% of the electricity currently generated by fossil fuel). We assume that $NO_x$ generated during the burning of $H_2$ can be controlled and $NO_x$ emissions remain unchanged. Lumped VOC emissions from electricity production represent ~1% of total Gidden 'Energy Production' emissions (Hoesly et al. (2018), which we assume to be negligible and leave unaltered. CO emissions from the Gidden 'Electricity' sectors are reduced by 10%. From Hoesly et al. (2018),

CO emissions from electricity represent 22% of emissions in the ‘Energy Production’ sector, therefore CO emissions in the Gidden ‘Energy Production’ sector are reduced by 2%.

To determine the associated reduction in $CH_4$ emissions in the Gidden ‘Energy Production’ sector, we assume that power consumption represents 39% of today’s total natural gas consumption (BP Energy Outlook, 2020), resulting in a reduction in fugitive emissions from natural gas of 11%. From UNFCCC data (https://unfccc.int/process-and-meetings/transparency-and-reporting/greenhouse-gas-data/ghg-data-unfccc/ghg-data-from-unfccc) fugitive emissions from natural gas represent 73% of combined fugitive gas and oil emissions, which in turn represents 58% of emissions in the Gidden ‘Energy Production’ sector. This leads to an overall reduction in $CH_4$ emissions in the Gidden ‘Energy Production’ sector of 5%. VOC emissions from the Gidden ‘Energy Production’ sector are also decreased by 5% following the calculated $CH_4$ reductions.

### 3.2.4 Summary of emission reductions

The emission reductions based on our global hydrogen economy scenario, determined the scaling factors described above are summarised in Table 2 to Table 5.

The calculated emission reductions for CO, $NO_x$ and VOCs are applied directly to the Gidden et al. (2019) emission data used in UKESM1. As $CH_4$ is implemented using a prescribed mixing ratio lower boundary condition in UKESM1, we use the atmospheric box model to convert our calculated $CH_4$ emission changes to a change in $CH_4$ mixing ratio to be used in the UKESM1 scenarios. Total global $CH_4$ emissions, including those from non-energy sectors, in the box model are 585 Tg $yr^{-1}$ (see Section 2.2), and therefore our calculated $CH_4$ emission reduction of 43 Tg $yr^{-1}$ represents a reduction in global $CH_4$ emissions of approximately 7%.

The expected reduction in carbon dioxide emissions based on the above hydrogen economy scenario and the Hoesly et al. (2018) emissions are shown in Table 5. Changes in carbon dioxide emissions are not considered in the UKESM1 scenarios, however they are discussed further in relation to the GWP determined for $H_2$ in Section 6.4.

**Table 2: Annual methane emission reductions**

| Energy Sector (Gidden et al., 2019) | Present Day Emissions (Gidden et al., 2019) (Tg $CH_4$) | Co-emission reductions (%) | Co-emission reductions (Tg $CH_4$) |
|---|---|---|---|
| Energy Production | 154 | 20 | 31 |

`Atmospheric implications of increased hydrogen use

| | | | |
|---|---|---|---|
| Transportation | 0.5 | 50 | 0.25 |
| Residential, Commercial, Other | 12 | 100 | 12 |
| TOTAL | 167 | 26 | 43 |

**Table 3: Annual carbon monoxide emission reductions**

| Energy Sector (Gidden et al., 2019) | Present Day Emissions (Gidden et al., 2019) (Tg CO) | Co-emission reductions (%) | Co-emission reductions (Tg CO) |
|---|---|---|---|
| Energy Production | 49 | 2 | 1 |
| Transportation | 149 | 50 | 74 |
| Residential, Commercial, Other | 245 | 75 | 184 |
| TOTAL | 443 | 58 | 259 |

**Table 4: Annual $NO_x$ emission reductions**

| Energy Sector (Gidden et al., 2019) | Present Day Emissions (Gidden et al., 2019) (Tg $NO_2$) | Co-emission reductions (%) | Co-emission reductions (Tg $NO_2$) |
|---|---|---|---|
| Energy Production | 34 | 0 | 0 |
| Transportation | 38 | 50 | 19 |
| Residential, Commercial, Other | 9 | 0 | 0 |
| TOTAL | 81 | 23 | 19 |

**Table 5: Annual carbon dioxide emission reductions**

| Energy Sector (Gidden et al., 2019) | Present Day Emissions (Gidden et al., 2019) (Tg $CO_2$) | Co-emission reductions (%) | Co-emission reductions (Tg $CO_2$) |
|---|---|---|---|
| Residential and Commercial | 10 | 100 | 10 |
| Transportation | 22 | 50 | 11 |
| Power Generation | 40 | 10 | 4 |
| Fugitive oil and gas | 1 | 34 | 0.4 |
| TOTAL | 73 | 34 | 25 |

## 3.3 Scenario Atmospheric Box Modelling

### 3.3.1 Relating changes in hydrogen emissions to changes in hydrogen mixing ratios

In our analysis of possible changes in $H_2$ emissions associated with a switch to a hydrogen economy we outline an illustrative future scenario of $H_2$ consumption where we estimate additional global $H_2$ emissions of between 9 and 96 Tg $yr^{-1}$ based on leakage rates of 1 and 10% respectively (see Table 1). The change in emissions could be substantially different to this due to uncertainty in the global proportion of energy consumption that $H_2$ will supply.

`Atmospheric implications of increased hydrogen use

Atmospheric box model simulations were performed using the coupled $H_2$-$CH_4$-CO-OH chemical scheme, as described in Section 2.2, to convert changes in $H_2$ emissions to changes in $H_2$ mixing ratio. Due to large uncertainties in how the soil sink of $H_2$ will respond to future changes in $H_2$ mixing ratios and climate, the box model simulations included two representations of the soil sink. In the first soil sink scenario, the soil sink is defined as a constant flux which does not change as $H_2$ mixing ratios increase. In the second soil sink scenario, a constant deposition velocity is used, so that the magnitude of the soil sink increases in line with $H_2$ mixing ratios. Figure 1 shows the increase in $H_2$ mixing ratio with increasing $H_2$ emissions in the box model, assuming a present day $H_2$ flux of 80 Tg $yr^{-1}$.

Based on the box model simulations, an increase in $H_2$ emissions of ~9 Tg $yr^{-1}$ would lead to an increase in $H_2$ mixing ratio of approximately 100 to 300 ppb, whilst an increase in $H_2$ emissions of ~96 Tg $yr^{-1}$ would lead to an increase in mixing ratio of ~600 to 4500 ppb, depending on the soil sink formulation. The uncertainty range in $H_2$ mixing ratios resulting from the different soil sink treatments is large, particularly for large changes in $H_2$ emissions. Experimental data suggests that the $H_2$ soil sink may be diffusion-limited rather than limited by biological activity, which would indicate that our constant deposition velocity (or 'inexhaustible sink') may be the more realistic scenario (Smith-Downey et al., 2008). In addition, a recent study by Paulot et al. (2021) concluded that the $H_2$ sink may increase by more than is suggested by our constant deposition velocity scenario in future due to changes in climate, potentially further limiting the increase in $H_2$ mixing ratios.

Based on these results, we chose to perform a range of hydrogen economy scenarios using $H_2$ mixing ratio lower boundary conditions of 750, 1000, 1500 and 2000 ppb (i.e., increases of approximately 250, 500, 1000 and 1500 ppb). We consider these values to span much of the uncertainty due to the ultimate size of the hydrogen economy, the $H_2$ soil sink and $H_2$ leakage rates. For example, taking a hydrogen economy of the size required to supply 23% of present day global energy consumption, and assuming the magnitude of the soil sink increases in line with the increase in $H_2$ mixing ratios (i.e. a constant deposition velocity), box model simulations indicate $H_2$ lower boundary conditions of 750, 1000 and 1500 ppb represent $H_2$ leakage rates of about 3, 7 and 13% respectively. However, these $H_2$ lower boundary conditions are also consistent with other fractions of total energy supplied by $H_2$, alternative soil sink responses and $H_2$ leakage rates. Example storylines for our largest $H_2$ LBC scenario, where the $H_2$ lower boundary condition is quadrupled to 2000 ppb, are outlined in Box 1. All storylines in Box 1 require a high-end assumption either related to the $H_2$ leakage rate, the ultimate size of a global hydrogen economy, or the soil sink response. Our 2000 ppb $H_2$ scenario should therefore be considered as an extreme end member designed to assess the linearity of the atmospheric response to increasing atmospheric $H_2$, rather than a prediction of potential future atmospheric $H_2$ levels in an $H_2$ economy.

**Box 1: Examples of storylines consistent with a 2000 ppb lower boundary condition for $H_2$:**

Storyline A: A global $H_2$ economy where $H_2$ provides 23% of global energy consumption (under present day levels), where the magnitude of the soil sink of $H_2$ increases linearly with $H_2$ mixing ratios (i.e. is deposited to soils with a constant deposition velocity) and where leakage rates of $H_2$ are very high (about 20%, exceeding current literature estimates).

Storyline B: A global $H_2$ economy where $H_2$ provides 23% of global energy consumption (under present day levels), but where the soil sink does not increase linearly with large increases in $H_2$ mixing ratios (i.e. it becomes limited by biological activity rather than by diffusion, see Figure 1). For a constant magnitude, fixed soil sink (black line, Figure 1) this storyline would correspond with an $H_2$ leakage rate of about 4%.

Storyline C: A global $H_2$ economy where $H_2$ provides a larger fraction of present day global energy consumption (or the same fraction of a larger future global energy demand), along with an $H_2$ leakage rate of less than 20%.

**Figure 1: The relationship between the total $H_2$ source and $H_2$ mixing ratios for two different representations of the $H_2$ soil sink: (i) a fixed sink that remains constant in magnitude at year 2000 values with varying $H_2$ mixing ratios (black line) and (ii) an inexhaustible $H_2$ sink that is based on a constant deposition velocity, where the magnitude of the soil sink increases linearly with increasing $H_2$ mixing ratios (red line).**

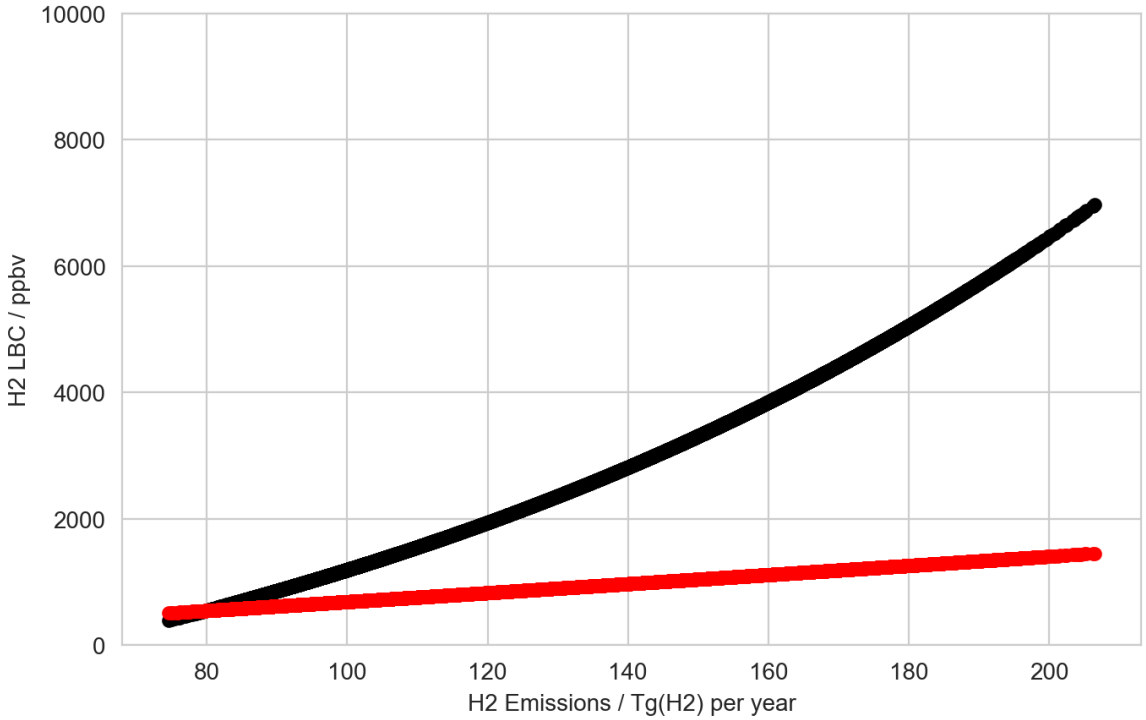

### 3.3.2 Relating changes in methane emissions to changes in methane mixing ratios

The explicit treatment of $CH_4$ emissions in UKCA is avoided due to the high computational cost associated with calculation of equilibrium climate states for species with long lifetimes. A spin-up time of more than 4 lifetimes (for $CH_4$ this is around additional 50 model years of computer simulations) is often required to determine equilibrium levels of these species. Our approach in the 3D chemistry-climate model uses the commonly adopted, more computationally efficient approach of a constant model lower boundary concentration, in which $CH_4$ levels are adjusted at each computational timestep to a prescribed value, chosen to represent the final, equilibrium or historical concentration.

We used the box model to calculate these lower boundary conditions for the 3D experiments presented here. Our approach was to use the computationally cheaper and lower complexity box model, driven by $CH_4$ emissions and realistic $CH_4$ loss rates and representative chemistry, to calculate final, equilibrium values of $CH_4$ for the various scenarios under consideration.

Our BASE experiment used year 2014 $CH_4$ levels of 1835 ppb, and our box model reproduced this level with emissions of 585 Tg($CH_4$) per year, consistent with literature estimates (Saunois et al., 2020). We examined the effect of $H_2$ emissions and reductions in species such as CO on $CH_4$ levels in this box modelling framework via the coupled $H_2$-$CH_4$-CO-OH chemical scheme above (Section 2.2).

In the first set of experiments, we examined the effect of reduced emissions of ozone precursor species such as $CH_4$ and CO on $CH_4$ levels. Whilst reductions in CO can lead to higher levels of OH, the main atmospheric sink of $CH_4$, we found that modelled $CH_4$ levels were relatively insensitive to changes in CO emissions and were determined primarily by the reduction in $CH_4$ emissions and the $H_2$ LBC. In our hydrogen economy scenario, we estimated global $CH_4$ emissions to be reduced by 7% (see Section 3.2). Our first experiment examines a 7% reduction in both $CH_4$ and CO emissions on $CH_4$ levels (in this case the 7% reduction in CO emissions is less than the reduction of ~20% indicated by our scenario analysis in Table 3). This leads to a reduction in modelled $CH_4$ mixing ratio of 182 ppb, which represents a 10% decrease in $CH_4$ relative to our BASE scenario (see Table 6).

A second scenario was investigated in which $H_2$ was increased by 1500 ppb to 2000 ppb $H_2$, while CO and $CH_4$ emissions were decreased by 7%. This simulation is particularly noteworthy as, despite the decrease in $CH_4$ emissions, $CH_4$ levels increased from 1835 ppb to 1961 ppb. This unexpected result arises from the effect of $H_2$ on the CO-$CH_4$-OH system. Higher levels of $H_2$, which functions as a sink for OH, thereby suppress the $CH_4$ chemical sink and higher levels of $CH_4$ result.

Finally, we examined a scenario in which $H_2$ levels increased without reductions in $CH_4$ or CO. In this case, the suppression of OH by $H_2$ leads to enhanced levels of $CH_4$ of 2171 ppb, an increase of 18%. Using simplified expressions for RF as a function of mixing ratio in e.g. Myhre et al. (1998) gives an additional 0.12 W $m^{-2}$ of clear-sky forcing (i.e. warming) by $CH_4$ forcing

under present day conditions of 330 ppb $N_2O$. We return to these results later. The $CH_4$ boundary conditions are summarised in Table 6.

**Table 6: A summary of methane lower boundary conditions determined by the box model and used in the UKESM1 simulations.**

| Box Model Scenario | Methane mixing ratio (ppb) |
|---|---|
| Base | 1835 |
| Base + methane emission reductions | 1652 |
| $H_2$(2000 ppb) + methane emission reductions | 1961 |
| $H_2$(2000 ppb) | 2171 |

## 3.4 UKESM1 simulations exploring the potential impacts of a hydrogen economy:

In this work, in addition to a base scenario, we consider four potential hydrogen economy scenarios based on the analysis above. A brief summary of each scenario is provided below. The lower boundary conditions for $H_2$ and $CH_4$ for each simulation are provided in Table 7, along with a description of the anthropogenic ozone precursor emissions.

BASE simulations: To calculate the impacts of a potential hydrogen economy, a simulation of the unmodified state of the atmosphere is required. In this work the BASE simulations take all boundary conditions from the recently developed CMIP6 dataset and assume a $H_2$ LBC of 500 ppb. Two BASE simulations have been performed, one at present day conditions, and one under future conditions. The present-day simulations use climatological boundary conditions for sea surface temperatures, sea ice extent and anthropogenic and natural emissions averaged over the years 2000-2014. This is done so that the present-day simulations represent average background conditions, rather than being representative of shorter-term fluctuation in climate or emissions (e.g., in response to the El Nino Southern Oscillation, [ENSO], large forest fires, etc). For the future simulations, these are run under 2050 conditions taken from the SSP2-4.5 scenario, with sea surface temperatures, sea ice extent and anthropogenic and natural emissions averaged over the years 2045-2055.

**Scenario 1: Changes to $H_2$ LBC only.** The most likely atmospheric response to any proposed hydrogen economy is a change in the atmospheric abundance of $H_2$. In this work, three simulations with increased $H_2$ surface mixing ratios have been performed, with $H_2$ LBCs of 750, 1000 and 2000 ppb at present day conditions. With the TS2014_BASE simulation this gives 4 simulations (TS2014_BASE, TS2014_750$H_2$, TS2014_1000$H_2$, TS2014_2000$H_2$) in which only the atmospheric abundance of $H_2$ is changed as an input, and the UKESM1 simulations can be used to explore the impacts of this single driver on atmospheric composition change. Under

future conditions we explore the atmospheric impacts of only the largest of these changes on ozone recovery using two simulations (TS2050_BASE and TS2050_2000$H_2$)

**Scenario 2: Reduced emissions of anthropogenic ozone precursors, excluding $CH_4$.** In addition to the expected changes to atmospheric $H_2$, any shift to a hydrogen economy is assumed to result in decreased emissions of CO, $NO_x$ and VOCs (sometimes here referred to as 'co-emissions') as the sources of these emissions are replaced with hydrogen alternatives (see Section 3.2.4 and Table 3 and Table 4). In this work we consider two scenarios with reduced ozone precursor emissions under present day conditions, the first with a $H_2$ LBC of 500 ppb (TS2014_O3Pre) and the second with a $H_2$ LBC of 2000 ppb (TS2014_2000$H_2$_O3Pre). TS2014_O3Pre represents a scenario with the ideal hydrogen economy in which anthropogenic emissions of ozone precursors are reduced with no corresponding change to the atmospheric abundance of $H_2$ (i.e., no $H_2$ leaks), while TS2014_2000$H_2$_O3Pre represents a scenario in which reductions in anthropogenic emissions of ozone precursors are associated with significant leaks from the $H_2$ infrastructure. An equivalent simulation to TS2014_2000$H_2$_O3Pre is also performed under future conditions (TS2050_2000$H_2$_O3Pre) to explore the impacts on ozone recovery.

**Scenario 3: $CH_4$ response to changes in atmospheric $H_2$.** An important atmospheric composition response to changes in atmospheric $H_2$ is the impact on $CH_4$. As the UKESM1 model uses LBCs to prescribe $CH_4$ mixing ratios at the surface, and the atmospheric lifetime of $CH_4$ is long, the tropospheric abundance of $CH_4$ in the UKESM1 model is highly constrained and does not respond significantly to changes in OH modelled in the Scenario 1 simulations. To evaluate the impact of changes to atmospheric $H_2$ on atmospheric $CH_4$ concentrations the box model was used to calculate new $CH_4$ LBCs that are consistent with the atmospheric composition changes seen in the scenario 1 simulations. TS2014_2000$H_2$_$CH_4$ therefore is a simulation with the same boundary conditions as TS2014_2000$H_2$, but the $CH_4$ LBC has been increased from 1835 ppb to 2171 ppb to account for the modelled effects of $H_2$ increases on atmospheric OH (see Section 3.3.2, Table 6). An equivalent simulation to TS2014_2000$H_2$ is also performed under future conditions (TS2050_2000$H_2$) to explore the impacts on ozone recovery.

**Scenario 4: Reduced emissions of anthropogenic ozone precursors, including $CH_4$.** In this final set of simulations, the changes considered in Scenarios 2 and 3 are combined alongside a reduction in $CH_4$ emissions: emissions of CO, $NO_x$ and VOCs are reduced (see Section 3.2, Table 3, Table 4), $CH_4$ emissions are reduced (see Table 2) and the surface abundance of $CH_4$ uses a value calculated with the box model to be consistent with both reductions in $CH_4$ emissions and composition changes resulting from changes to atmospheric OH. For present day conditions we consider two simulations, TS2014_O3Pre_1652$CH_4$ in which emissions of CO, $NO_x$, $CH_4$ and VOCs are reduced but with no change in the $H_2$ LBC (i.e., no $H_2$ leaks) and TS2014_2000$H_2$_O3Pre_1961$CH_4$ which has the same reductions in emissions but also includes an increase in the $H_2$ LBC to 2000 ppb.

All simulations performed as part of this work are so-called timeslice simulations which are run for multiple decades using annually repeating boundary conditions (i.e., the sea surface temperatures, sea ice extent, anthropogenic and natural emissions, land use configuration, etc.

are the same every year of the simulation). The result of this is many years with the same forcings but which start with slightly different atmospheric states, providing some estimate of the variability. The UKESM1 simulations evaluated in this work were each run for 40 years, with the final 25 years of each simulation used for analysis and the initial 15 years treated as a spin-up period. This spin-up is required for the surface changes to the $H_2$ LBC, the $CH_4$ LBC and/or the emissions of anthropogenic ozone precursors to propagate to higher altitudes. In the stratosphere, slow transport via the Brewer-Dobson circulation results in surface changes taking 7-10 years to reach the polar lower stratosphere. 15 years spin-up time allows this slow circulation to get through 1.5-2 overturning cycles, and as a result the surface changes affect all levels of the modelled atmosphere. In some circumstances, such as the calculation of radiative forcing and global warming potentials, the transient response to a change is required, and this can be calculated using data from the spin-up.

The results from these integrations are presented in the following sections. Section 4 considers changes in atmospheric composition in the troposphere and stratosphere, while their effect on radiative forcing is discussed in Section 5.

**Table 7: List of hydrogen economy simulations using UKESM1.**

| Experiment | $H_2$ LBC (ppb) | $CH_4$ LBC (ppb) | Anthropogenic ozone precursors |
|---|---|---|---|
| **Present Day (2014) Timeslice Experiments** | | | |
| TS2014_BASE | 500 | 1835 | 2000-2014 climatology from CMIP6 historical |
| TS2014_750$H_2$ | 750 | 1835 | As TS2014_BASE |
| TS2014_1000$H_2$ | 1000 | 1835 | As TS2014_BASE |
| TS2014_1500$H_2$ | 1500 | 1835 | As TS2014_BASE |
| TS2014_2000$H_2$ | 2000 | 1835 | As TS2014_BASE |
| TS2014_1500$H_2$_2058$CH_4$ | 1500 | 2058 | As TS2014_BASE |
| TS2014_2000$H_2$_2171$CH_4$ | 2000 | 2171 | As TS2014_BASE |
| TS2014_O3Pre | 500 | 1835 | Reduced $O_3$ precursor emissions |
| TS2014_1500$H_2$_O3Pre | 1500 | 1835 | Reduced $O_3$ precursor emissions |
| TS2014_2000$H_2$_O3Pre | 2000 | 1835 | Reduced $O_3$ precursor emissions |
| TS2014_O3Pre_1652$CH_4$ | 500 | 1652 | Reduced $O_3$ precursor emissions |
| TS2014_1000$H_2$_O3Pre_1756 $CH_4$ | 1000 | 1756 | Reduced $O_3$ precursor emissions |
| TS2014_2000$H_2$_O3Pre_1961 $CH_4$ | 2000 | 1961 | Reduced $O_3$ precursor emissions |
| **Future (2050) Timeslice Experiments** | | | |
| TS2050_BASE | 500 | 2020 | 2045-2055 climatology from CMIP6 SSP2-4.5 |
| TS2050_2000$H_2$ | 2000 | 2020 | As TS2050_BASE |
| TS2050_2000$H_2$_2395$CH_4$ | 2000 | 2395 | As TS2050_BASE |
| TS2050_2000$H_2$_O3Pre | 2000 | 2020 | Reduced $O_3$ precursor emissions |
| TS2050_2000$H_2$_O3Pre_2156 $CH_4$ | 2000 | 2156 | Reduced $O_3$ precursor emissions |

# 4 Atmospheric Composition

Increases to atmospheric $H_2$ have the potential to affect atmospheric composition in both the troposphere, where changes may impact air quality, and the stratosphere, where changes may impact stratospheric ozone recovery (e.g. Tromp et al., 2003; Schultz et al., 2003; Warwick et al., 2004). Additionally, these changes have associated climate impacts. In the following section we explore the impacts of increases to atmospheric $H_2$ and associated reductions in CO, $NO_x$, VOCs and $CH_4$ emissions reductions outlined in the scenarios described in Section 3. All analysis presented here evaluates climatological responses averaged over the last 25 years of the model simulations. In all figures showing differences between two simulations, only those differences that are statistically significant at the 95% confidence level, calculated using a two-tail student t-test, are shown. For the calculation of tropospheric amount, we used a dynamic tropopause, calculated online as in Archibald et al. (2020).

## 4.1 Impacts of a hydrogen economy on atmospheric composition:

### 4.1.1 Hydroxyl Radical, Methane and Hydrogen lifetime:

Figure 2 shows the zonal mean impact of increasing only atmospheric $H_2$ on OH mixing ratios. Decreases in OH are modelled throughout the troposphere, with larger decreases in scenarios with higher $H_2$ abundances. The change in OH is linear in $H_2$ when other emissions are held constant; for every 1ppm increase in $H_2$, tropospheric mean OH decreases by about $0.90 \times 10^5$ molecules $cm^{-3}$ (when including the $CH_4$ feedback on its own lifetime, see Figure 4A, below). In the TS2014_2000$H_2$ scenario, in which surface mixing ratios of $H_2$ increase to 2000 ppb, modelled OH decreases by more than 10%. A reduction in OH with increasing atmospheric $H_2$ is consistent with R1 being the main atmospheric sink for $H_2$:

$$H_2 + OH \rightarrow H_2O + H \qquad \text{(R1)}$$

In contrast to reductions in tropospheric OH, stratospheric OH is modelled to increase with increasing atmospheric $H_2$ as in the stratosphere $H_2$ reacts with energetically excited oxygen atoms to produce OH:

$$H_2 + O(^1D) \rightarrow OH + H \qquad \text{(R5)}$$

Additionally, OH is formed in the stratosphere through reaction of $O(^1D)$ with water vapour and $CH_4$:

$$H_2O + O(^1D) \rightarrow 2OH \qquad \text{(R6)}$$

$$CH_4 + O(^1D) \rightarrow OH + CH_3 \qquad \text{(R7)}$$

**Figure 2: Zonal mean OH mixing ratios for the TS2014_BASE simulation (A), and percentage differences with respect to the TS2014_BASE simulation for the TS2014_750$H_2$ simulation (B), TS2014_1000$H_2$ simulation (C), and TS2014_2000$H_2$ simulation (D). Results shown are averages from the final 25 years of the model simulations; only differences that are statistically significant at the 95% confidence level are presented.**

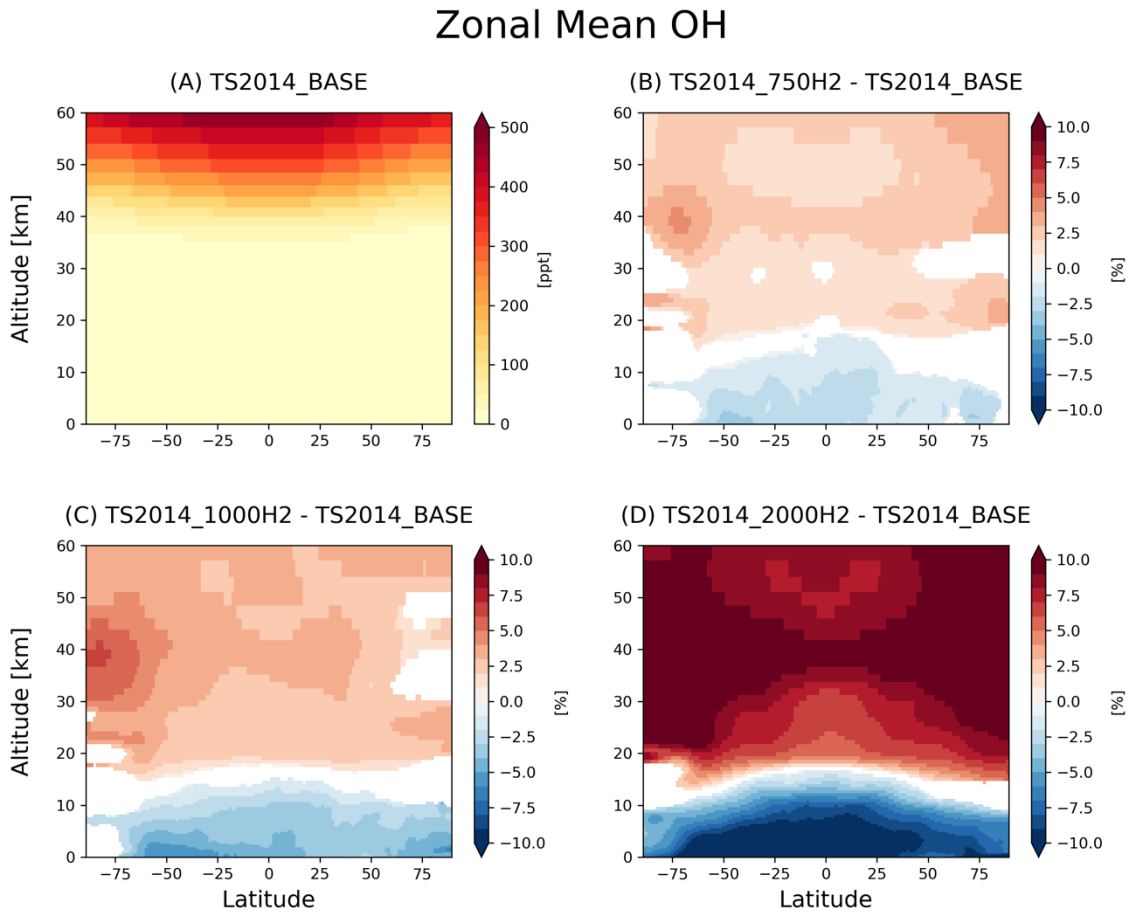


Figure 3 shows the zonal mean water vapour response to increases in atmospheric $H_2$. The mixing ratio of water vapour in the troposphere is controlled by the hydrological cycle (evaporation from the oceans, precipitation, etc). The impact from chemical reactions on tropospheric water vapour is ignored. However, in the extremely dry stratosphere, where $H_2O$ mixing ratios are less than 10 ppm, chemical sources of water vapour are very important. Figure 3 shows that stratospheric water vapour mixing ratios increase with increasing $H_2$, with increases of up to 25% (> 1 ppm) in the TS2014_2000$H_2$ scenario.

Reductions in tropospheric OH are expected to result in increases in atmospheric $CH_4$; the major atmospheric sink of $CH_4$ is through reaction with OH.

$$CH_4 + OH \rightarrow CH_3 + H_2O \qquad \text{(R2)}$$

However, as discussed in Section 2.1, the UKESM1 model prescribes $CH_4$ lower boundary conditions, and so this chemical response of $CH_4$ to changes in atmospheric $H_2$ is not included in the TS2014_750$H_2$, TS2014_1000$H_2$, and TS2014_2000$H_2$ scenarios. Instead, to identify the impacts on $CH_4$ of $H_2$-induced tropospheric OH reductions we use a chemical box model (see Sections 2.2 and 3.3.2). The box modelling work indicates that for an increase in surface

`Atmospheric implications of increased hydrogen use

$H_2$ mixing ratios to 2000 ppb, surface $CH_4$ mixing ratios will increase from 1835 ppb to 2171 ppb (Table 6).

**Figure 3: Zonal mean $H_2O$ mixing ratios for the TS2014_BASE simulation (A), and percentage differences with respect to the TS2014_BASE simulation for the TS2014_750$H_2$ simulation (B), TS2014_1000$H_2$ simulation (C), and TS2014_2000$H_2$ simulation (D). Results shown are averages from the final 25 years of the model simulations; only differences that are statistically significant at the 95% confidence level are presented.**

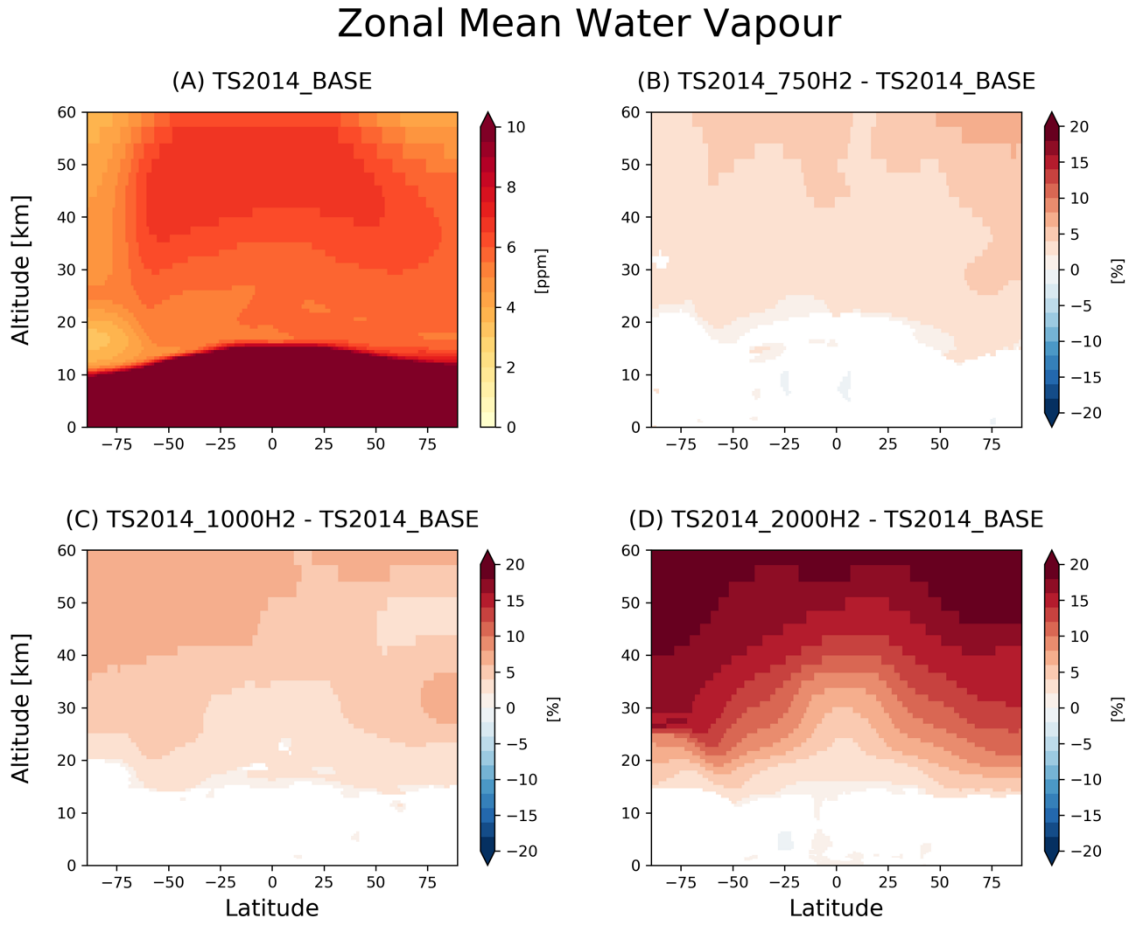


Together, the increases to stratospheric $H_2$, $H_2O$ and $CH_4$ identified above significantly increase stratospheric production of OH through increases in the rates of reactions R5, R6 and R7, which offset any changes to reaction R1 and result in increased stratospheric OH mixing ratios. Changes to stratospheric water vapour and $HO_x$ radicals have potential impacts on stratospheric ozone recovery that will be explored in Section 4.3.

While changes to atmospheric $H_2$ have a direct impact on tropospheric OH, as shown in Figure 2, associated changes in $CH_4$ and reductions in the emissions of CO, $NO_x$, VOCs and $CH_4$ following a shift to a global hydrogen economy also have the potential to impact tropospheric OH. Figure 4A shows the airmass weighted tropospheric mean OH (a measure of the average tropospheric changes) plotted as a function of $H_2$ LBC. For all scenarios, as atmospheric $H_2$ increases, tropospheric OH decreases. However, the magnitude of this decrease is dependent upon not just the changes to $H_2$, but also on changes to $CH_4$ and the emissions of ozone precursors.

**Figure 4: (A) Mass weighted tropospheric mean OH plotted as a function of the $H_2$ surface mixing ratio. The black dashed line is the fit through the experiments in which $CH_4$ responds to changing atmospheric $H_2$ (and OH). (B) $H_2$ chemical lifetime with respect to OH plotted as a function of the mass weighted tropospheric mean OH. The black dashed line is the fit through all experiments. (C) $CH_4$ lifetime plotted as a function of the $H_2$ surface mixing ratio. The black solid line is the fit through experiments in which only $H_2$ is changing. The black dashed line is the fit through the experiments in which $CH_4$ responds to changing atmospheric $H_2$ (and OH). (D) $CH_4$ chemical lifetime with respect to OH plotted as a function of the mass weighted tropospheric mean OH. The black dashed line is the fit through all experiments.**

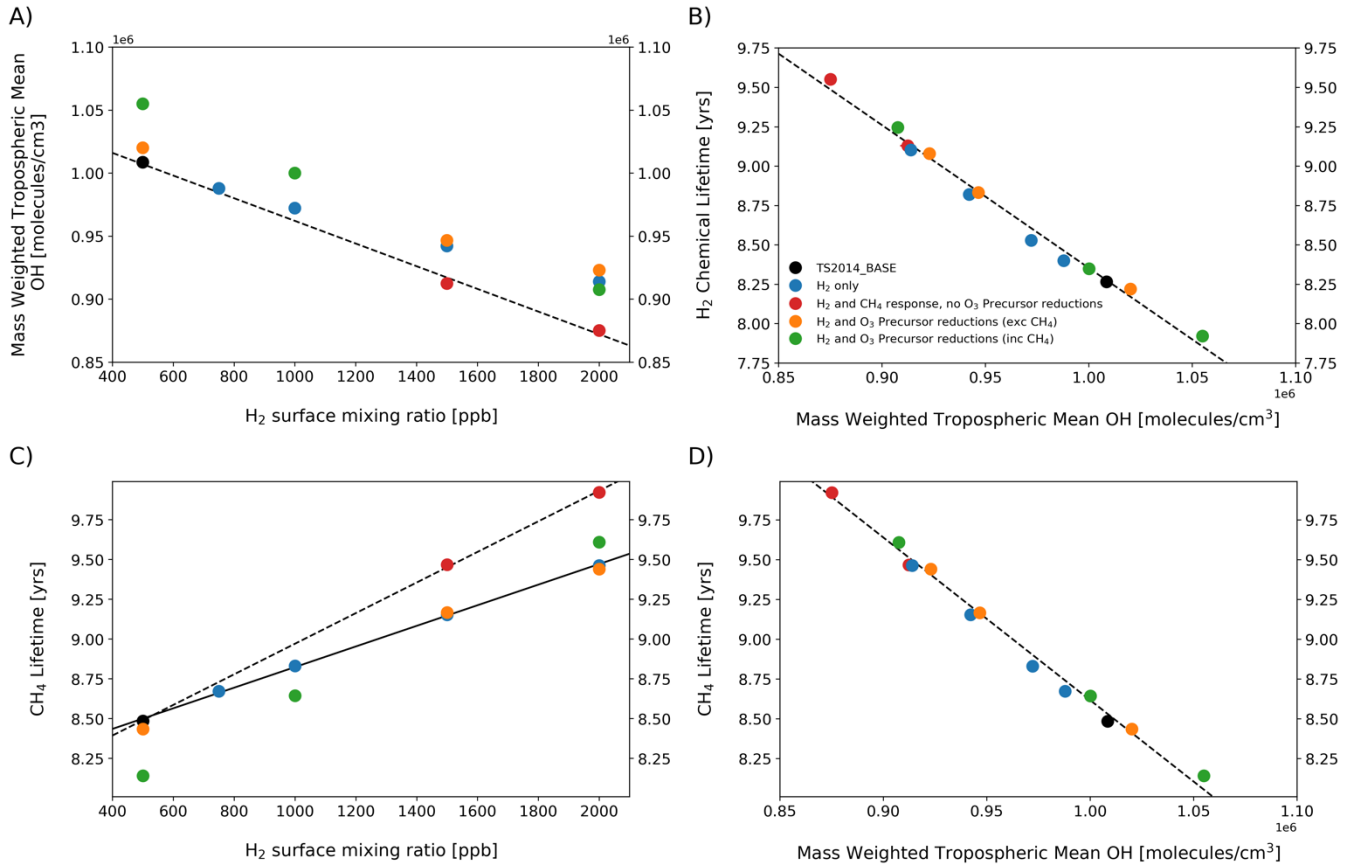


Reductions in tropospheric OH lead to increases to atmospheric $CH_4$. The red points in Figure 4 include the anticipated increase in $CH_4$ mixing ratios resulting from an increase in atmospheric $H_2$ with no change in $CH_4$ or VOC emissions. When the impacts of $H_2$ increases on $CH_4$ are considered, tropospheric mean OH decreases by a larger amount than when this feedback is ignored (blue points) due to an increase to the flux through reaction R2.

Anticipated reductions in the emissions of CO, $NO_x$ and VOCs associated with a shift to a hydrogen economy have a negligible impact on tropospheric mean OH (compare blue and orange points, Figure 4A). In contrast, when anticipated reductions in $CH_4$ emissions are also considered (green points), significant increases (~5%) in tropospheric OH are modelled for scenarios with low $H_2$ surface mixing ratios (i.e., low assumed $H_2$ leakage). For the largest atmospheric $H_2$ mixing ratios considered in this study (i.e., high assumed $H_2$ leakage), the assumed ~7% reduction to $CH_4$ emissions is enough to offset the expected decrease in OH resulting from the $CH_4$ feedback described above, and as a result the blue and green points at

2000 ppb $H_2$ have similar tropospheric mean OH concentrations. Clearly, the response of OH and $CH_4$ to a shift to a hydrogen economy is complex. Keeping atmospheric $CH_4$ mixing ratios low requires a decrease in both emissions of $CH_4$ and a limit on how much $H_2$ is emitted to the atmosphere.

The climate impacts of $H_2$ will depend on its atmospheric lifetime and on how leakage of $H_2$ affects the atmospheric lifetime of $CH_4$. In the TS2014_BASE simulation, the UKESM1 modelled $H_2$ lifetime with respect of OH is 8.3 years. As atmospheric $H_2$ increases and tropospheric OH decreases, the chemical sink for $H_2$ is reduced, and its lifetime with respect to OH increases. This feedback between the atmospheric abundance of $H_2$, tropospheric OH and the chemical lifetime of $H_2$ is similar to that previously mentioned for $CH_4$ (see Section 2.2). However, since for $H_2$ the soil sink is larger than the OH chemical sink, this chemical feedback has a smaller impact on the total atmospheric lifetime of $H_2$ than for $CH_4$.

As discussed above, increasing atmospheric $H_2$ results in decreased tropospheric OH concentrations. This increases the lifetime of $CH_4$, which has important consequences for climate. Figure 4 shows the $CH_4$ lifetime as a function of atmospheric $H_2$ and tropospheric OH. In the 2014_BASE simulation, the modelled $CH_4$ lifetime is 8.5 years, which is in good agreement with other studies. As atmospheric $H_2$ increases but all other factors remain constant, there is a linear increase in the $CH_4$ lifetime of 0.64 years for every 1 ppm increase in $H_2$. However, decreased tropospheric OH concentrations also lead to increases in the $CH_4$ burden. When this change is also considered, the $CH_4$ lifetime increases by 0.96 years for every 1 ppm increase in $H_2$.

### 4.1.2 Carbon Monoxide

The potential impacts of a global shift to a hydrogen economy include reductions in atmospheric CO and $NO_x$ associated with reductions in various emissions sectors (see Section 3.2). Together, these relatively short-lived species play an important role in the chemical production of ozone and are often termed (alongside $CH_4$ and VOCs) ozone precursors.

Surface mixing ratios of CO are spatially heterogeneous (Figure 5A), with a distribution governed by the location of CO emissions. These emissions include both natural and anthropogenic sources, and consequently CO mixing ratios are highest in regions with large population densities or that experience significant wildfires. As atmospheric $H_2$ increases but all other factors remain constant (i.e., ozone precursor emissions and atmospheric $CH_4$ concentrations) tropospheric CO mixing ratios increase globally, with larger increases modelled in the southern hemisphere (Figure 5B). This response is driven by the decreases to OH discussed in Section 4.1.1; the main chemical sink of CO is reaction with OH, and increases in atmospheric $H_2$ decrease OH mixing ratios, thereby reducing that loss.

**Figure 5: Surface CO mixing ratio for the TS2014_BASE simulation (A), and percentage differences with respect to the TS2014_BASE simulation for the TS2014_2000$H_2$ simulation (B) and TS2014_2000$H_2$_O3Pre_1961$CH_4$ simulation (C). Results shown are averages from the final 25 years of the model simulations; only differences that are statistically significant at the 95% confidence level are presented.**

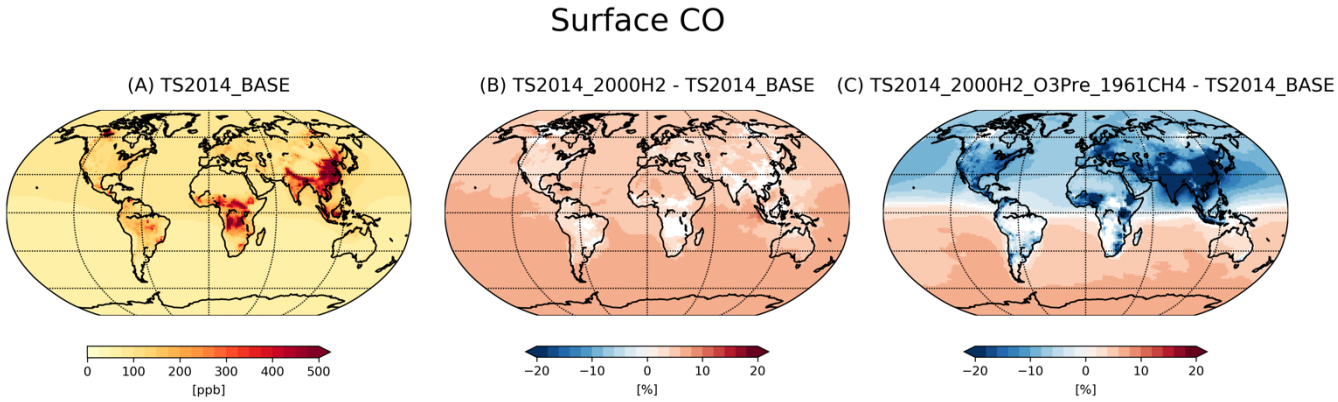


A more complex response is seen in CO when changes to ozone precursor emissions and atmospheric $CH_4$ are considered. Decreases to ozone precursor emissions in the absence of any other changes result in strong decreases to surface CO mixing ratios, particularly in those areas close to large anthropogenic emissions sources, with additional decreases when $CH_4$ emissions are also reduced (not shown). However, when the effects of reduced co-emissions and increased atmospheric $H_2$ are considered together, a clear hemispheric difference in the CO response is seen (Figure 5C). In the more polluted Northern Hemisphere, the impact of local ozone precursor emissions reduction dominates and CO mixing ratios decrease. In contrast, in the less polluted Southern Hemisphere, reductions to OH dominate the CO response, resulting in increased CO mixing ratios.

### 4.1.3 Ozone

#### Tropospheric Ozone

Tropospheric ozone is not directly emitted, and its atmospheric abundance instead reflects a balance between downward transport from the stratosphere, deposition at the surface and the difference between chemical production and loss processes. Photochemical production of ozone is driven by oxidation of carbon monoxide (CO), methane ($CH_4$) and volatile organic compounds (VOCs) in the presence of the oxides of nitrogen. As a result, the OH, $NO_x$ and CO changes identified above all contribute to the tropospheric ozone response to changes in atmospheric $H_2$ abundance.

Modelled annual mean tropospheric column ozone values and the tropospheric column ozone response to changes in atmospheric $H_2$ abundance as well as ozone precursors are shown in Figure 6. In general, tropospheric column ozone increases as atmospheric $H_2$ increases, particularly in the tropics and Northern Hemisphere midlatitudes (although small decreases, not statistically significant, are modelled between the simulations with 500 and 750 ppb $H_2$ at the surface). Figure 6B shows that for an increase of $H_2$ from 500 ppb to 2000 ppb, tropospheric column ozone increases, with a global mean increase of 0.59 DU. The increases

to tropospheric ozone are driven primarily through increases in the reaction $HO_2$ + NO, which increases by ~7% when atmospheric $H_2$ increases to 2000 ppb.

**Figure 6: Tropospheric column ozone for the TS2014_BASE simulation (A), and differences with respect to the TS2014_BASE simulation for the TS2014_2000$H_2$ simulation (B) and TS2014_2000$H_2$_O3Pre_1961$CH_4$ simulation (C). Results shown are averages from the final 25 years of the model simulations; only differences that are statistically significant at the 95% confidence level are presented.**

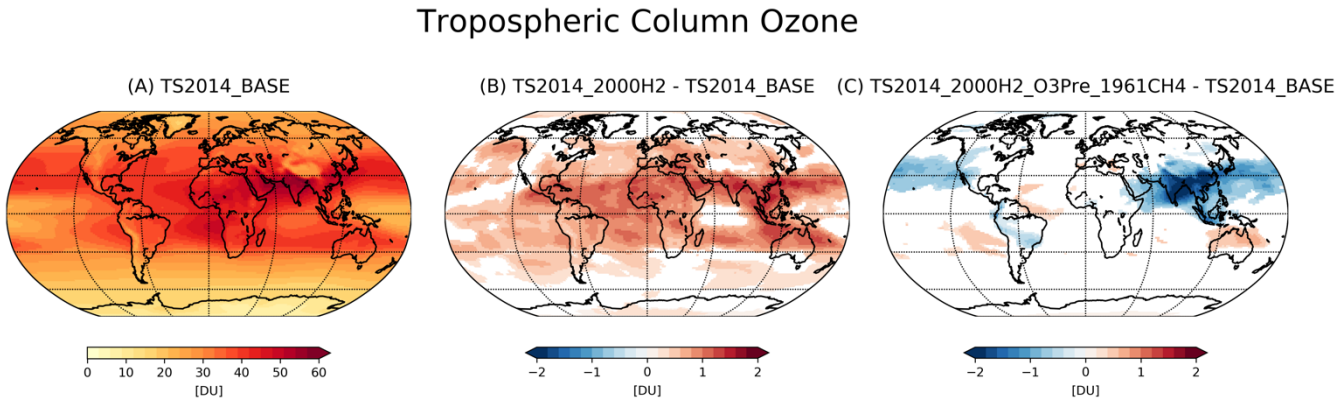


However, when atmospheric $CH_4$ increases, the effect is to enhance the tropospheric ozone column increase. In contrast, when reductions in ozone precursor and $CH_4$ emissions are considered, tropospheric column ozone decreases. The tropospheric ozone response to a global shift towards a hydrogen economy is therefore strongly influenced by the amount of $H_2$ added to the atmosphere through leaks, and the co-benefit reductions achieved in CO, $NO_x$, non-methane hydrocarbon and $CH_4$ emissions. In a UKESM1 simulation which assumes a large $H_2$ leakage, with surface mixing ratios of $H_2$ reaching 2000 ppb, and emissions reductions in CO, $NO_x$, non-methane hydrocarbon and $CH_4$ emissions (following the assumptions presented in Section 3.2), the global mean tropospheric column ozone response is found to be small (-0.1 DU) due to the competing effects outlined above (Figure 6C).

Figure 7 shows the tropospheric ozone burden for each of the simulations used in this report, plotted as a function of the $H_2$ surface mixing ratio (i.e., a measure of the amount of $H_2$ escaping to the atmosphere). Different coloured points in Figure 7 separate the experiments into groups: the base simulation (black); simulations in which only $H_2$ is increasing (blue); simulations in which $CH_4$ responds to the increasing $H_2$ (i.e., $CH_4$ increases; red); simulations in which the ozone precursor emissions ($NO_x$, CO and VOCs) are reduced (orange); and simulations in which the ozone precursor emissions (including $CH_4$) are reduced (green). As atmospheric $H_2$ increases so too does the tropospheric ozone burden. For an increase in atmospheric $H_2$ of 1 ppm, in the absence of any other changes (blue points), the tropospheric ozone burden increases by 4.7 Tg (black solid line**,** Figure 7). When increases to $CH_4$ in response to decreasing OH mixing ratios are also considered, there is a stronger tropospheric ozone response, with the tropospheric ozone burden increasing by 12.1 Tg per 1 ppm increase in $H_2$ (black dashed line**,** Figure 7). The change in tropospheric ozone for a given change in $H_2$ is not dependent on the background ozone precursor/$CH_4$ field. This is evidenced by the fact that the slope through the orange/green points matches that through the blue/red points.

`Atmospheric implications of increased hydrogen use

The tropospheric ozone response to a potential hydrogen economy is dependent on several uncertain factors (e.g., the size of the hydrogen economy, the leakage rate, the associated reductions in other anthropogenic species). The linear relationships shown in Figure 7 allow the ozone change for a range of different emission scenarios for $H_2$ and $CH_4$ to be estimated, giving the tropospheric ozone response to any future hydrogen economy.

**Figure 7: Tropospheric ozone burden plotted as a function of the $H_2$ surface mixing ratio. The black solid line is the fit through the experiments in which only $H_2$ is changing. The black dashed line is the fit through the experiments in which $CH_4$ responds to changing atmospheric $H_2$ (and OH). The grey solid/dashed lines show the same slope as the black solid/dashed lines, but moved to line up with the orange/green points respectively, in order to highlight that the same linear relationship holds for different ozone precursor emissions.**

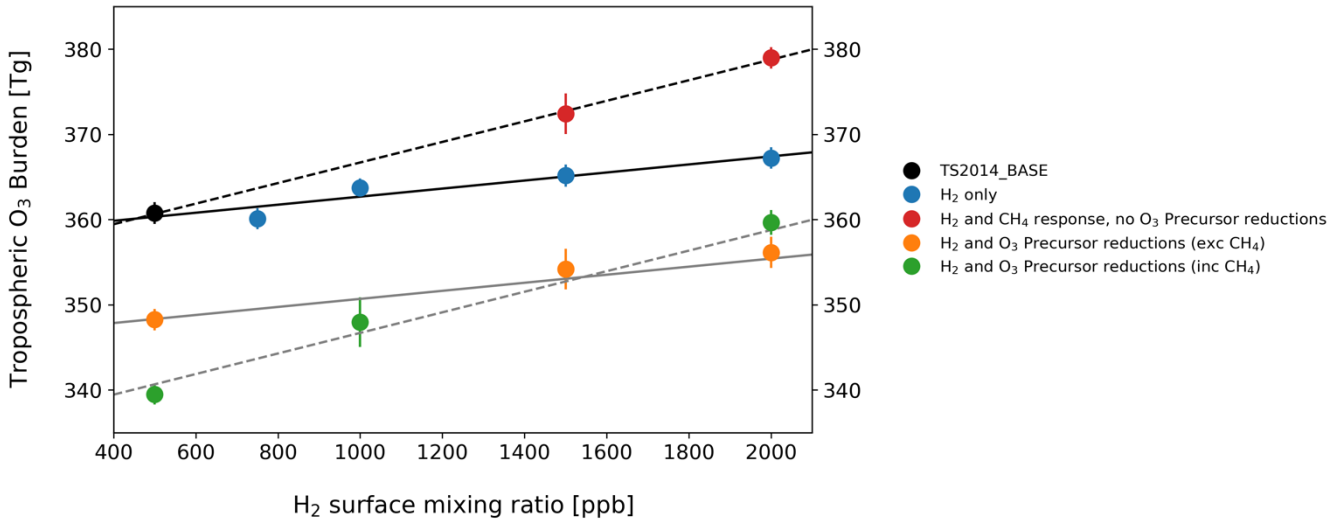


## Stratospheric ozone

In contrast to tropospheric ozone, stratospheric ozone is produced through photochemical reactions involving molecular and atomic oxygen, and destroyed through catalytic reactions involving $ClO_x$, $BrO_x$, $HO_x$, and $NO_x$ radicals. As seen above, a shift to a hydrogen economy will result in increased stratospheric water vapour mixing ratios (Figure 3). This has the potential to modify the stratospheric ozone depletion, particularly those reactions involving $HO_x$ radicals, and also to change stratospheric temperatures. Lower temperatures and increased stratospheric water vapour can lead to increased formation of polar stratospheric clouds, enhancing polar ozone depletion. Therefore, investigating the stratospheric ozone response to increased atmospheric $H_2$ is key.

Annual mean, zonal mean ozone mixing ratios and total column ozone climatologies are shown in Figure 8 for the TS2014_BASE simulation along with differences for the TS2014_2000$H_2$ and TS2014_2000$H_2$_2171$CH_4$ simulations with respect to TS2014_BASE. As discussed in Section 4.1.1, as atmospheric $H_2$ increases, so too does tropospheric ozone, and this increase is further enhanced when the $CH_4$ response is considered. In contrast, ozone in the upper stratosphere and polar lower stratosphere decreases with increasing atmospheric $H_2$, while in the lower and middle stratosphere of mid-latitudes and the tropics ozone mixing ratios remain relatively unchanged.

**Figure 8: Top row: zonal mean ozone mixing ratios for the TS2014_BASE simulation (A), and percentage differences with respect to the TS2014_BASE simulation for the TS2014_2000$H_2$ simulation (B), and TS2014_2000$H_2$_2171$CH_4$ simulation (C). Bottom row: total column ozone climatology for the TS2014_BASE simulation (D), and differences with respect to the TS2014_BASE simulation for the TS2014_2000$H_2$ simulation (E), and TS2014_2000$H_2$_2171$CH_4$ simulation (F). Results shown are averages from the final 25 years of the model simulations; only differences that are statistically significant at the 95% confidence level are presented.**

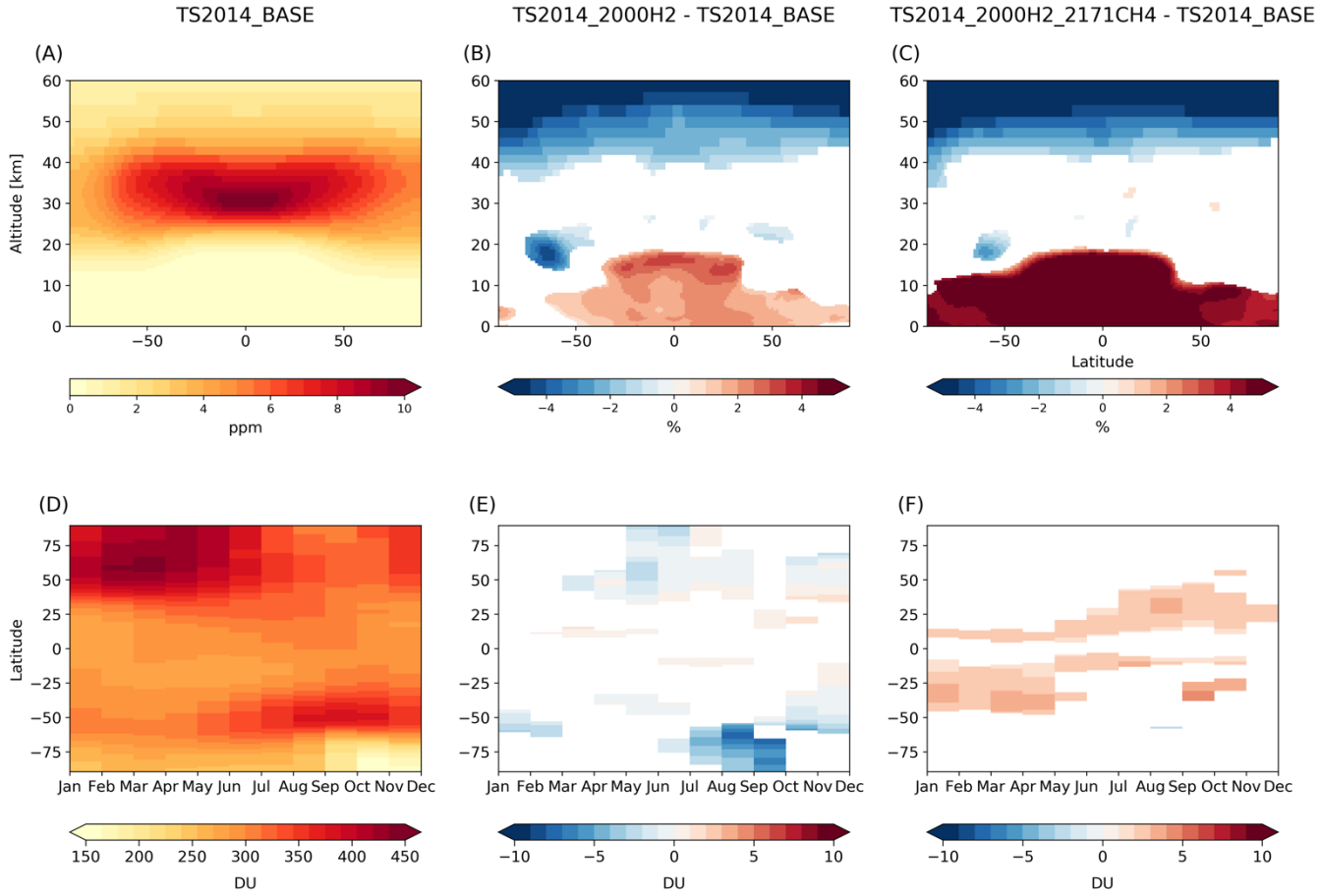


When the total ozone column climatology is considered (lower row in Figure 8), the largest decreases are modelled in the Antarctic springtime, indicating increased polar lower stratospheric ozone depletion with increased atmospheric $H_2$ (Figure 8E). However, these changes, while statistically significant, are relatively small (5-10 DU). When the $CH_4$ response to increasing atmospheric $H_2$ mixing ratios is considered, no statistically significant total column ozone depletion is modelled (Figure 8F), with some small (up to 5 DU) increases in mid-latitude and tropical total column ozone. It should be remembered that the total column includes changes to tropospheric ozone, and that this small increase seen in Figure 8F is driven by the large increases to tropospheric ozone mixing ratios shown in Figure 8C and discussed above.

## 4.2 Sensitivity of tropospheric ozone changes to background climate

Figure 9 shows annual mean tropospheric column values for both the TS2014 and TS2050 base simulations (panels A and B). As discussed above, the 2050 simulations are performed using 2045-2055 climatological boundary conditions taken from the CMIP6 SSP2-4.5 scenario. Also shown is the tropospheric column ozone response to an increase in atmospheric $H_2$ (panels C and D) and to an increase in atmospheric $H_2$ in conjunction with reductions in tropospheric ozone precursors (panels E and F). Under both present and future climate conditions, tropospheric column ozone is modelled to increase in response to increased atmospheric $H_2$ mixing ratios. The spatial pattern of this increase is broadly consistent under the two climate states, with largest increases between 30ºS-30ºN. The magnitude of this increase is also broadly consistent with a global mean tropospheric column ozone increase of 0.59 DU under present day conditions and 0.76 DU under future climate conditions for a 1500 ppb increase in $H_2$. Similarly, when reductions in ozone precursor emissions and the response of atmospheric $CH_4$ changes are considered alongside increases to atmospheric $H_2$, the spatial pattern of tropospheric column ozone changes are consistent between the two climate states. For both, large decreases are modelled over South and Southeast Asia, with smaller decreases throughout much of the Northern Hemisphere as these regions have the largest reductions in anthropogenic ozone precursor emissions, while small increases in tropospheric column ozone are modelled in the Southern Hemisphere. Global mean tropospheric column ozone is modelled to reduce by 0.1 DU under present day conditions, and 0.25 DU under 2050 conditions. This analysis indicates that there is not a significant difference in the modelled response of tropospheric ozone to potential emissions changes associated with a $H_2$ economy under the different climate states considered here.

**Figure 9: Tropospheric column ozone in the BASE simulations (top row) and response to increased atmospheric $H_2$ mixing ratio (middle row) and increased $H_2$ mixing ratios with reductions in anthropogenic ozone precursors and associated changes to atmospheric $CH_4$ (bottom row) under present day (2014) and future (2050 SSP2-4.5) climate states. Results shown are averages from the final 25 years of the model simulations; only differences that are statistically significant at the 95% confidence level are presented.**

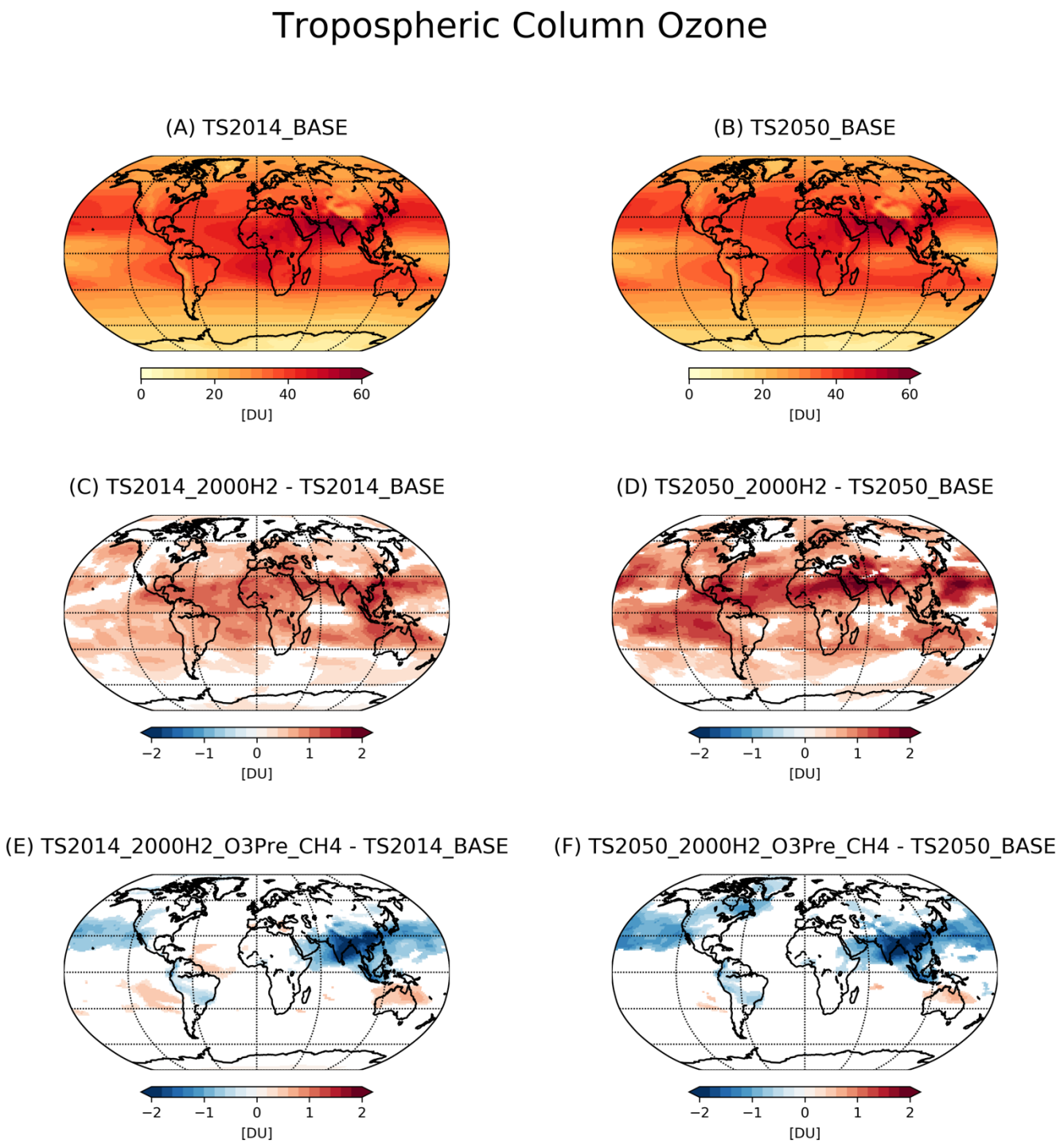

## 4.3 Impacts of a hydrogen economy on ozone recovery

Figure 10 shows the evolution of annual mean total column ozone, averaged over 60°S-60°N, from 1960 to 2100 following the SSP2-4.5 scenario. This data is taken from UKESM1 simulations performed as part of the CMIP6 activity. The long-term evolution of total column ozone follows a well understood pathway: large, rapid declines from 1970 to the late 1990s associated with the emission of chlorinated ozone depleting substances (principally chlorofluorocarbons such as CFC-11 and CFC-12), followed by slow recovery as stratospheric chlorine declines in the future. Plotted over this timeseries are data from the timeslice experiments used in this study. Good agreement is seen between the year 2014 and year 2050 base timeslice simulations (blue circles) and the CMIP6 timeseries. For both time periods, increased atmospheric $H_2$, in the absence of any other changes, leads to small decreases in total column ozone. When changes to atmospheric $CH_4$ are also considered, total column ozone increases slightly. However, the total column ozone response to changing atmospheric $H_2$, with and without the associated changes to atmospheric $CH_4$, are within the spread of the CMIP6 ensemble (denoted by the orange envelope). This indicates that even large changes in atmospheric $H_2$ will likely have a negligible impact on ozone recovery. The only simulations in which significant changes to total column ozone are modelled are those 2050 simulations which consider reductions in tropospheric ozone precursors. As discussed above, total column ozone changes include those in the troposphere, and reductions to ozone precursors reduce the tropospheric ozone burden. However, the stratospheric ozone changes resulting from these emissions reductions are not significant.

**Figure 10: Total column ozone projections from 1960-2100, averaged over 60ºS-60ºN, following the SSP2-4.5 scenario performed by the UKESM1 model for CMIP6. The black line shows the ensemble mean, and the orange envelope shows the ensemble spread. Also shown are timeslice experiments performed as part of this work for the present day (2014) and future (2050) scenarios.**

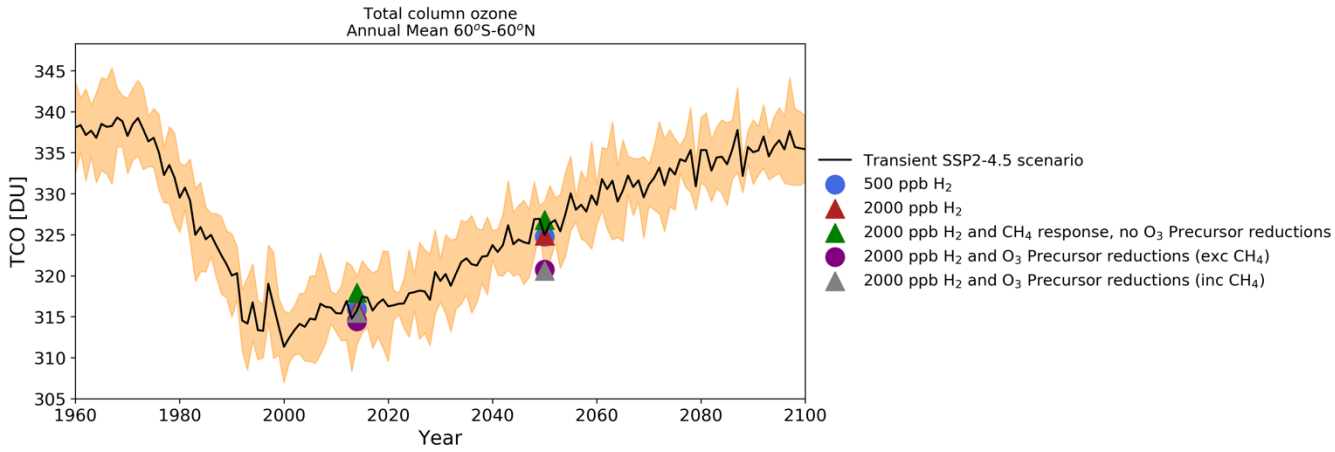

# 5 Radiative forcing

## 5.1 Overview

The impact of $H_2$ emissions on the Earth's energy budget involves a number of pathways, chiefly through modification of the levels of radiatively important gases such as ozone and $CH_4$, and modification of gas-phase oxidant levels which then alters the level of aerosols (so-called 'direct' aerosol effect) and the properties of clouds formed by these aerosol particles ('indirect' aerosol effects).

In this section, we present the Effective Radiative Forcing (ERF) for each of the scenarios studied relative to the Base experiment. Our choice of ERF (IPCC 2014; IPCC 2021) as a metric allows the climate forcing of $H_2$ to be compared with other composition and Earth system changes in a consistent manner. The ERF concept incorporates rapid adjustments to e.g. clouds and water vapour that occur independent of surface temperature change. The UKESM1 allows the effect of these adjustments to be estimated and for this study, we used the methods detailed in O'Connor et al. (2020). This change in radiative forcing can be related approximately to the global mean equilibrium surface temperature change via

$$\Delta T \approx \lambda \Delta F$$

in which $\Delta F$ is ERF, and $\Delta T$ the temperature change. $\lambda$, the constant of proportionality, is around +0.86 K per W $m^{-2}$; a positive change in radiative flux leads to an increase in surface temperature. $\Delta F$ is calculated as the sum of both shortwave and long wavelength regions.

Note that in the following we have not included the significant climate benefit arising from the reduction in $CO_2$ emissions which should follow a move to $H_2$. We are simply looking at the radiative forcing which would result from changes to $H_2$ in the atmosphere.

**Figure 11: The effect of the simulated changes in atmospheric composition on effective radiative forcing (ERF). Left hand panel shows the ERF as a function of $H_2$ and other experimental conditions; right hand figure shows the ERF as a function of $CH_4$ and other experimental conditions.**

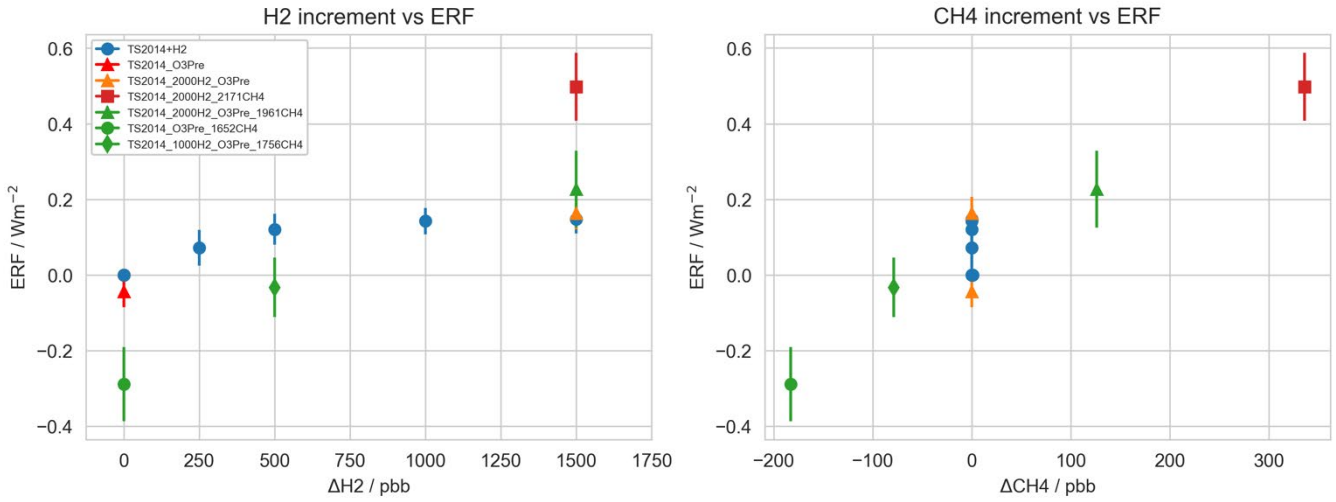


Figure 11 summarises the ERF for the various experiments, labelled according to the $H_2$ and $CH_4$ lower boundary mixing ratios and, if appropriate, whether ozone precursor emissions were decreased.

The ERF varies from cooling (negative ERF) to warming (positive ERF) tendency depending on the scenario. The largest ERF occurs for the largest increases in $H_2$. The data in Figure 11 suggest the sensitivity of ERF to changing $H_2$ levels is greatest for small changes in $H_2$, but there is a large uncertainty on the ERF and further work is required to diagnose the factors controlling sensitivity in the ERF response. Similarly, the larger the increase in $CH_4$, the larger is the ERF; conversely, the larger the decrease in $CH_4$, the greater the climate benefit (the more negative the ERF). Reductions in the emissions of ozone precursors (triangles in Figure 11) generally have a small impact on radiative forcing for the scenarios considered (but would have a significant air quality benefit).

Increases in $H_2$ are driven by its leakage into the atmosphere. Figure 11 shows that for maximum climate benefit it is essential to limit any leakage of $H_2$ to a minimum. As explained further below, this reduces any increase in the concentrations (and radiative forcing) of tropospheric ozone or stratospheric water vapour; it also mitigates against the potential increase in the $CH_4$ lifetime with, again, a climate benefit.

We explore these ERFs in more detail in the following sections, focussing first in Section 5.2 on the experiment where the $H_2$ LBC changed to 2000 ppb, with no other changes (experiment TS2014_2000$H_2$) and in Section 5.2 on the experiment where we assume no $H_2$ leakage but with the $CH_4$ LBC reduced to 1652 ppb (experiment TS2014_O3Pre_1652$CH_4$).

## 5.2 Impacts of increased hydrogen levels on radiative forcing

The forcing, $\Delta F$, can be broken down into the radiative impact of gas-phase species, so-called clear-sky effects, and the changes to the radiative properties of clouds, in both short- and long wavelength regions. Clouds serve to cool the planet, and so changes in cloud properties can affect the ERF via modifications to planetary albedo in the visible region, and also via changes to the outgoing long wavelength radiation.

Figure 12 shows the ERF broken down into short and long wavelength regions, and clear-sky and cloud radiative effects for experiment TS2014_2000$H_2$, relative to the base experiment. The global mean changes are small, about 0.14 W $m^{-2}$ compared to an historical $CO_2$ forcing of 1.8 W $m^{-2}$, but statistically significant (see Figure 12). The variability of the radiative fluxes, which is the result of internal (natural) model variability, is of the order of 0.1 W $m^{-2}$. Figure 12 also shows the ERF as a function of latitude and longitude. In this case, a mask has been applied to occlude regions where the ERF is within the statistical variation of the modelled flux at that location, and only regions where the signal is above this are plotted.

Figure 12 shows large regional variations. In this experiment, the largest changes are in the longwave clear-sky forcing, consistent with increased levels of tropospheric ozone and stratospheric water vapour, radiatively important gases, and in cloud radiative properties in the short wavelength region.

**Figure 12: ERF for TS2014_2000$H_2$ calculated with respect to BASE. CRE denotes cloud radiate effect. A mask has been applied to remove data from the plot where the ERF is less than the model ERF interannual variability.**

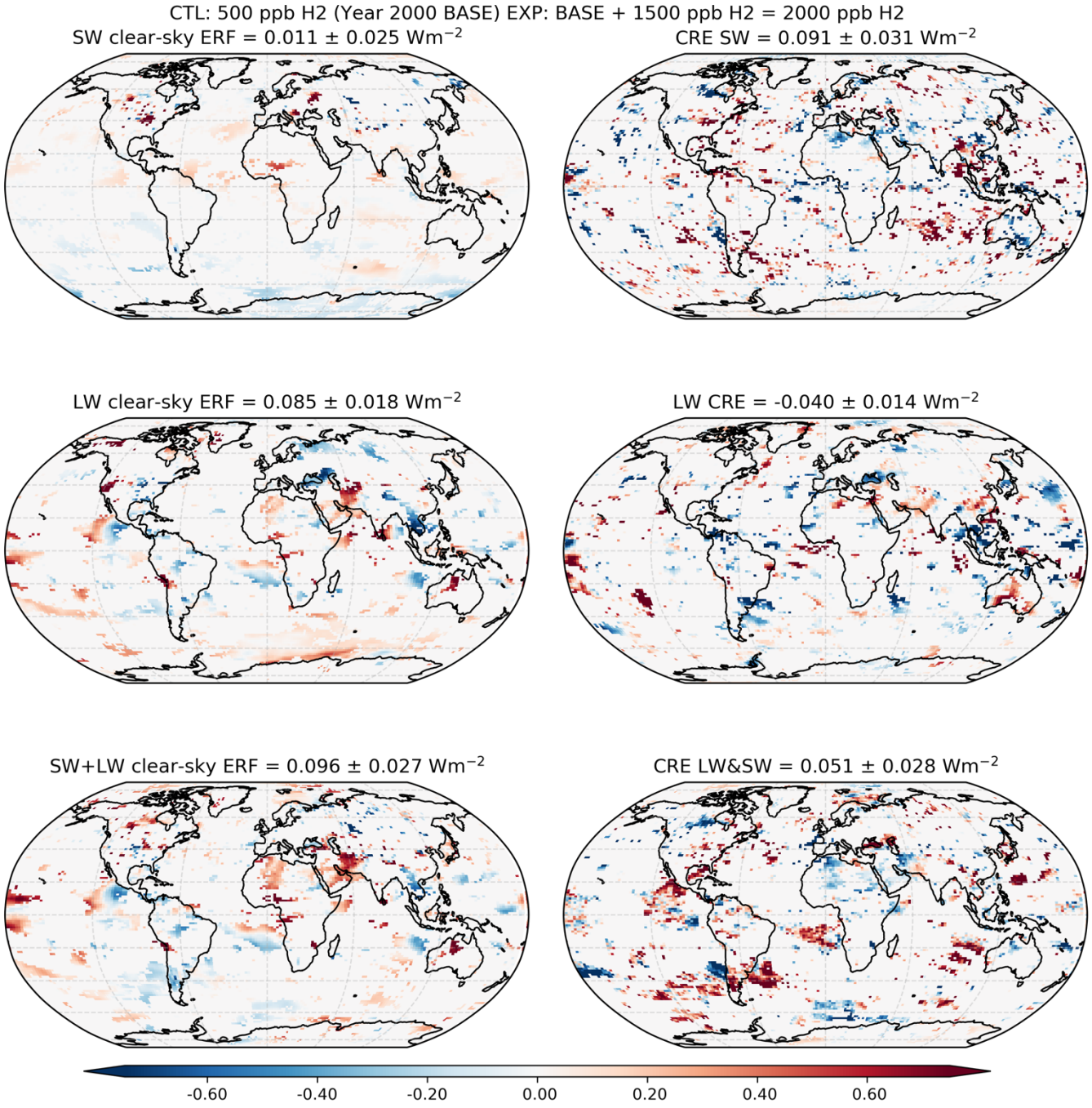

**Figure 13: Cloud droplet number concentration (CDNC) in the UKESM1 model at 1km altitude. The left hand figure shows CDNC in the base (500 ppb $H_2$ case), the right hand the change in CDNC when $H_2$ is increased to 2000 ppb.**

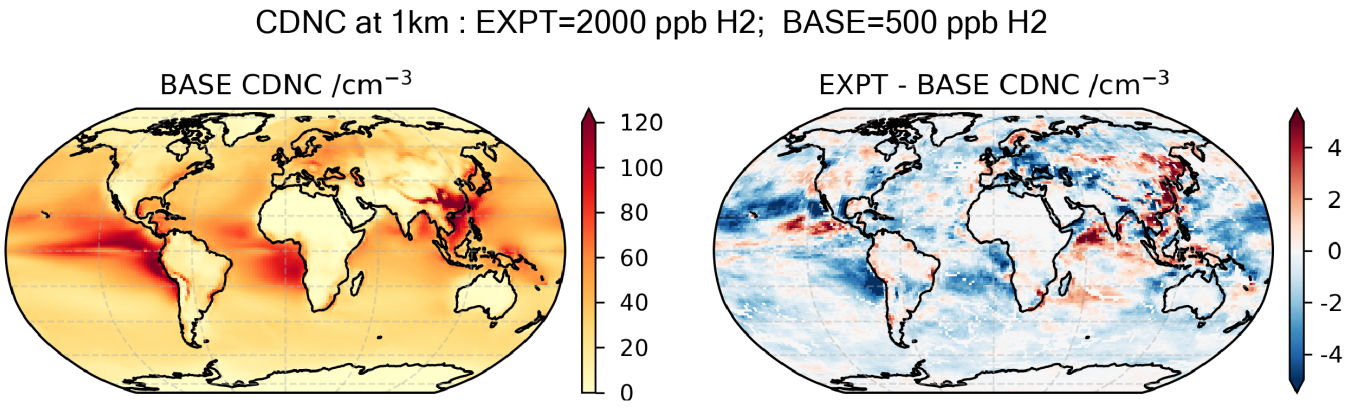


Figure 13 shows for the same experiments the change in the cloud droplet number concentration (CDNC), a key property governing the reflectivity of the cloud. The cloud albedo is closely tied to droplet number (Twomey, 1959; IPCC 2014; 2021); a cloud with a larger CDNC will, for a given condensable water amount, have smaller individual droplets which more efficiently scatter light at visible wavelengths, making the cloud more reflective. The figure shows that increasing $H_2$ levels in the atmosphere results in a reduction in CDNC and hence a lower cloud albedo. The decrease in reflected light serves as a positive radiative forcing in the short wavelength region, and so would be expected to lead to an increase in global mean surface temperature (GMST). While future work would examine the full climate response, the methods employed here serve to determine the climate forcing, which ultimately drives the climate response.

We ran a further experiment to quantify the effect of simultaneous reductions in emissions of ozone precursors in comparison with TS2014_2000$H_2$. Within statistical uncertainty, the resulting ERF (TS2014_2000$H_2$_O3Pre) was identical to that from the TS2014_2000$H_2$ experiment described above. Similarly, an experiment in which ozone precursors were reduced relative to the base experiment (in this case without any change in the $H_2$ LBC) also led to a change in ERF that was not statistically significant.

## 5.3 Radiative forcing and Methane

A further group of experiments examined the radiative effect of changes in $CH_4$ levels, in response either to changes in the $CH_4$ emissions or as a response to changing levels of the gas phase oxidant, OH, consequent on $H_2$ emissions as discussed in Section 4.

Our first experiment in this group examined the $CH_4$ response to suppression of the OH sink. In scenario TS2014_2000$H_2$_2171$CH_4$, we examined the effect of $H_2$ on $CH_4$ levels in the present day. We allowed $CH_4$ levels to adjust to new equilibrium values consistent with the decreased OH levels that result from increased $H_2$ emissions. This equilibrium value is significantly higher than present day levels, by around 340 ppb, and illustrates the impact of $H_2$ on the coupled

OH-$CH_4$-$H_2$ system. The increase in $CH_4$ results in a strong forcing of nearly 0.5 W $m^{-2}$ (see Figure 11), an additional 0.35 W $m^{-2}$ over the BASE+1500 ppb $H_2$ case in which $CH_4$ levels were held at present day levels. This ERF is significantly larger than the clear-sky forcing estimated using simplified expressions for RF in section 3.3, and illustrates the importance of additional contributions to the RF, such as cloud adjustments. In the second experiment in this set, TS2014_2000$H_2$_O3Pre_1961$CH_4$, we examined the effect of a combined increase in $H_2$, which decreases OH and the $CH_4$ sink, and expected decreases in emissions of both $CH_4$ and O3PRE from present-day levels (see Section 3.2). Despite the decrease in $CH_4$ emissions, $CH_4$ equilibrium levels are 1961 ppb, higher than the BASE case of 1835 ppb, illustrating the effect of $H_2$ on OH levels. As shown in Figure 11, in this experiment the ERF was 0.23 W $m^{-2}$, higher than the BASE+1500ppb $H_2$ case, highlighting the expected role of $CH_4$ in the climate response.

In the third experiment, TS2014_O3Pre_1652$CH_4$, the scenario reflects a decline in $CH_4$ emissions from a switch to $H_2$ as a fuel source (see Section 3.2), with simultaneous decrease in ozone precursor emissions. In this scenario, $H_2$ emissions are tightly controlled and the $H_2$ level remains at 500 ppb. $CH_4$ levels fall along with tropospheric ozone and stratospheric water vapour. This scenario results in a significant negative ERF of 0.3 W $m^{-2}$ (Figure 11) or a cooling of approximately 0.26 °C.

Figure 14 shows that the ERF response in this case is complex and distributed more-or-less evenly across shortwave cloud response (decreased $CH_4$ leads to increased OH, which leads to increased CDNC, as with, but in the opposite sense to, the TS2014_2000$H_2$ experiment), and a large decrease in LW CS forcing, presumably due to decreases in $CH_4$ and $O_3$, with a more complex long wavelength cloud response that may be the result in a change of cloud top height due to the significant change in cloud properties.

The ERFs calculated in these latter experiments are similar in magnitude to the results from a study by Paulot et al. (2021), who found an ERF of 0.17 $Wm^{-2}$ in their HIGH_$H_2$_$CH_4$ experiment, in which $H_2$ emissions were 200 Tg per year and $CH_4$ levels had been raised from 1808 ppb to 2005 ppb, an increase of 197 ppb. In the UKCA model, assuming linearity of response in Figure 11, a 197 ppb increase in $CH_4$ would lead to an ERF of approximately 0.24 $Wm^{-2}$, about 40% higher than that calculated using the GFDL-AM4.1 model used in Paulot et al. (2021). This higher sensitivity of ERF to increases in $CH_4$ mixing ratio in UKESM has been noted elsewhere (see, e.g., O'Connor et al. (2021)), and reflects the cascade of changes in oxidants that result from changes in $CH_4$ (and $H_2$) – which go on to affect aerosols and clouds. Such couplings and feedbacks are relatively unique in UKESM compared with other CMIP6 models, but more studies are required to constrain the magnitude of the response of aerosols to changes in oxidants.

**Figure 14: ERF for TS2014_O3Pre_1652$CH_4$ calculated with respect to BASE. The $CH_4$ decreases result in large decrease (cooling) in LW CS; OH increases (Strat $H_2O$ decreases) lead to enhanced cloud albedo (increased stratospheric $O_3$) and negative forcing.**

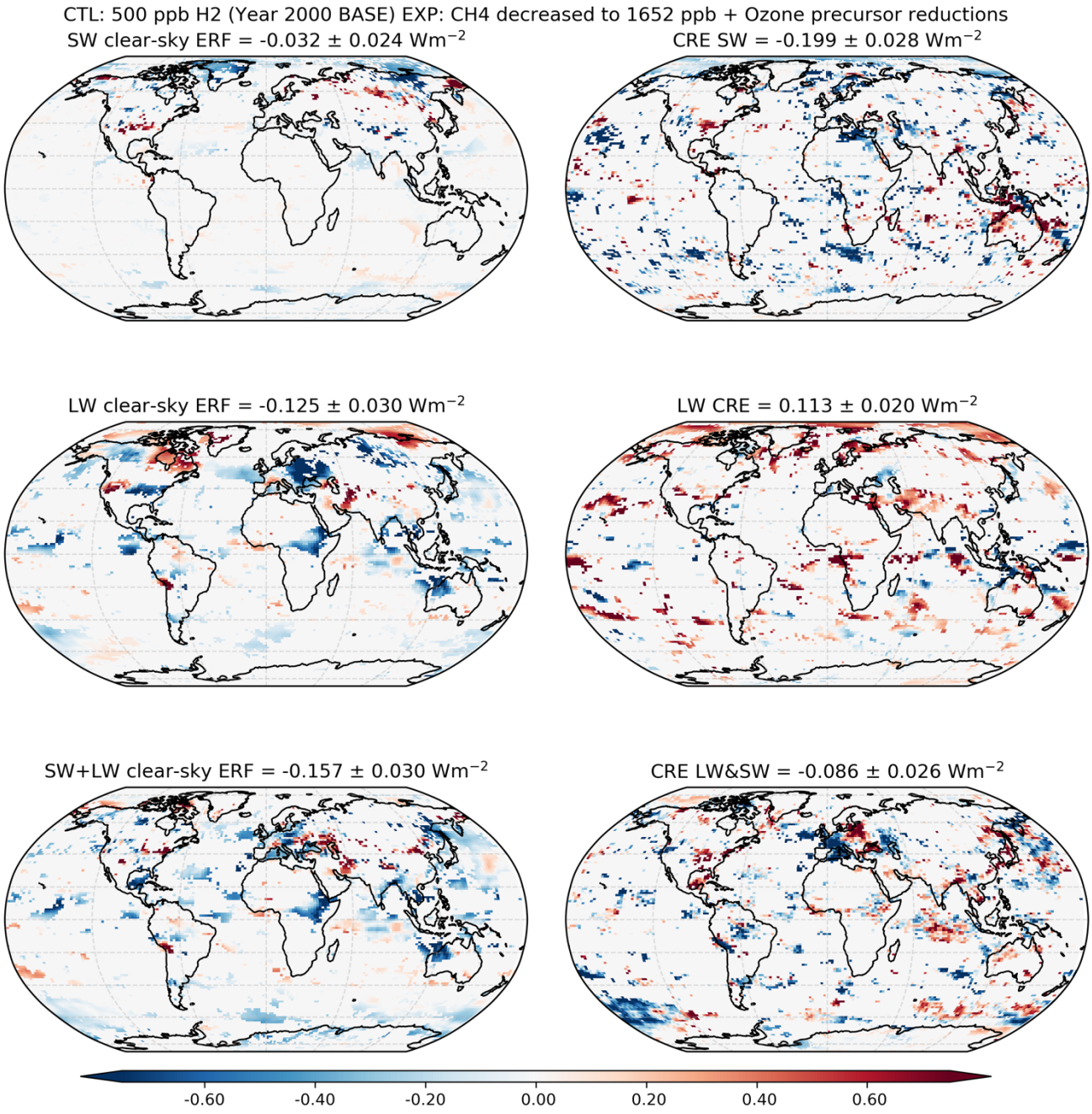


Table 8 summarises the radiative forcing changes resulting from the full set of experiments conducted.

**Table 8: Summary of atmospheric composition and radiative forcing changes in experiments (where Tau $CH_4$ is the methane lifetime).**

| Experiment | OH | TAU $CH_4$ | Trop $O_3$ | ERF Clear Sky LW + SW | ΔCRE LW + SW | ERF all sky, LW+SW |
|---|---|---|---|---|---|---|
| | $10^6$ $cm^{-3}$ | Years | Tg | W $m^{-2}$ | W $m^{-2}$ | W $m^{-2}$ |
| Base | 1.22 | 8.48 | 360.8 | N/A | N/A | N/A |
| TS2014_750$H_2$ | 1.20 | 8.67 | 360.1 | 0.051 ± 0.041 | 0.021 ± 0.041 | 0.0722± 0.095 |
| TS2014_1000$H_2$ | 1.18 | 8.83 | 363.7 | 0.069 ± 0.054 | 0.033 ± 0.054 | 0.102 ± 0.097 |
| TS2014_2000$H_2$ | 1.11 | 9.46 | 367.2 | 0.096 ± 0.056 | 0.051 ± 0.056 | 0.148 ± 0.076 |
| TS2014_O3Pre | 1.24 | 8.43 | 348.2 | -0.0021 ± 0.053 | -0.051 ± 0.053 | -0.053 ± 0.077 |
| TS2014_2000$H_2$_O3Pre | 1.11 | 9.43 | 356.1 | 0.110 ± 0.056 | 0.054 ± 0.044 | 0.164 ± 0.087 |
| TS2014_2000$H_2$_O3Pre_1961$CH_4$ | 1.09 | 9.60 | 359.7 | 0.186 ± 0.108 | 0.0404 ± 0.108 | 0.223 ± 0.202 |
| TS2014_O3Pre_1652$CH_4$ | 1.27 | 8.14 | 339.5 | -0.16 ± 0.14 | -0.123 ± 0.104 | -0.289 ± 0.196 |
| TS2014_2000$H_2$_2171$CH_4$ | 1.06 | 9.92 | 379.0 | 0.342 ± 0.099 | 0.155 ± 0.104 | 0.497 ± 0.179 |

# 6 Calculation of the Global Warming Potential

## 6.1 Background

A global warming potential (GWP) quantifying the indirect radiative forcings associated with $H_2$ has so far only previously been determined in a very limited number of studies (Derwent et al., 2020, an update on Derwent et al., 2006, and Field and Derwent, 2021). Using a 3-dimensional global chemistry-transport model, Derwent et al. (2020) obtained a GWP(100) (100 year time horizon GWP) for $H_2$ of $5 \pm 1$. Field and Derwent (2021) obtained a value of $3.3 \pm 1.4$ using a 2-dimensional tropospheric model. Both of these studies considered only the influence of $H_2$ on tropospheric composition ($CH_4$ and ozone) in their $H_2$ GWP estimates, excluding any contribution from potential changes in the stratosphere.

The indirect radiative forcing associated with $H_2$ was calculated by Paulot et al. (2021) using a chemistry-climate model incorporating both changes in tropospheric and stratospheric composition, but they did not determine an $H_2$ GWP. One third of their estimated total indirect forcing due to $H_2$ (0.84 mW $m^{-2}$/($TgH_2\,yr^{-1}$)) is attributed to the stratospheric response associated with an increase in water vapour, highlighting the potential importance of the stratosphere for an $H_2$ GWP. To our knowledge, our study here is the first study to determine a GWP for $H_2$ including both the tropospheric and stratospheric response.

## 6.2 Method: determining GWPs from steady-state simulations

The GWP is defined as the cumulative radiative forcing over a specified time horizon resulting from the emission of a unit mass of gas relative to a reference gas ($CO_2$). GWPs can be derived from either transient model simulations, which follow the chemical and forcing evolution of a pulse emission, or from steady-state simulations, together with additional information about the lifetimes of the chemical perturbations following a step emission. As both $H_2$ and $CH_4$ chemical tracers in UKESM1 use a defined concentration lower boundary condition, we employ the steady-state method to determine a GWP for $H_2$.

Fuglestvedt et al. (2010) describe a method by which steady-state simulations can be employed to derive GWPs from indirect forcings. Their methodology was adopted to present GWPs for short-lived climate forcers in the IPCC Fifth Assessment Report (IPCC, 2014) and implicitly adopted for Global Temperature Change Potentials in the IPCC Sixth Assessment Report (IPCC, 2021). However, we found this method to be unsuitable for use with species with intermediate atmospheric lifetimes, such as $H_2$. As part of this study, we derive a more universal version of the equations presented in Fuglestvedt et al. (2010), suitable for use with $H_2$. This method and our $H_2$ GWP calculations based on UKESM1 results are outlined in Annex 1.

## 6.3 Atmospheric lifetime of molecular hydrogen

The atmospheric lifetime of $H_2$ is an important, but uncertain, factor in determining the GWP for $H_2$. It is determined by fluxes through two main destruction pathways: reaction with the hydroxyl radical (OH) and uptake by soils. Uptake by soils is estimated to represent ~75% of $H_2$ destruction, with the remainder due to reaction with OH. The overall lifetime of atmospheric $H_2$ ($\alpha_H$) is represented by:

$$\frac{1}{\alpha_H} = \frac{1}{\tau_{H2+OH}} + \frac{1}{\tau_{H2SOIL}}$$

Where $\tau_{H2+OH}$ is the lifetime of $H_2$ with respect to the OH sink and $\tau_{H2SOIL}$ is the lifetime of $H_2$ with respect to soil uptake. There are uncertainties in both lifetimes, however the majority of the uncertainty in the $H_2$ lifetime is due to uncertainty in the soil uptake lifetime (e.g. Ehhalt and Rohrer 2009). This is relevant for GWP calculations as the magnitude of the soil sink determines the relative proportion of any future $H_2$ leakage that will be taken up by soils, compared to that which will react with OH in the atmosphere, subsequently inducing chemical feedbacks and indirect radiative forcings. In our study, the total $H_2$ lifetime, $\alpha_H$, is derived from UKESM1 results combined with existing literature studies. As $H_2$ is prescribed as a lower boundary condition in UKESM1, we can determine a chemical lifetime for $H_2$ based on reaction with OH within the model, but not an $H_2$ lifetime with respect to uptake by soils. The $H_2$ lifetime used in our GWP calculations is therefore based on the chemical lifetime derived from UKESM1 in our TS2014_BASE simulation (8.3 years) and a range of soil uptake lifetimes taken from published global $H_2$ budget model studies. We use this range of values to account for the influence of soil sink uncertainties on the $H_2$ GWP (Novelli et al., 1999; Yashiro et al., 2011; Hauglustaine and Ehhalt, 2002; Sanderson et al., 2003; Rhee et al., 2006; Xiao et al., 2007; Price et al., 2007; Ehhalt and Rohrer, 2009; Pieterse et al., 2013; Paulot et al., 2021; see Table 9). This results in a range for $\alpha_H$ of 1.4 to 2.2 years, with a mid-range estimate of 1.9 years.

Uncertainties in the chemical lifetime of $H_2$ are not considered in the GWP calculation as they will be correlated with uncertainties in other relevant parameters (e.g. the $CH_4$ lifetime) and therefore simulations with multiple models and chemistry schemes would be required to assess their impact on the GWP. However, we note that due to the dominance of the soil sink, uncertainties in the chemical sink have a minor impact on the total $H_2$ lifetime (relevant for the GWP calculation). For example, when the range of chemical $H_2$ lifetimes from existing literature studies (listed above) is combined with a mean soil uptake lifetime of 2.5 years, this results in a range in the total $H_2$ lifetime of 1.9 to 2.0 years, significantly less than the range resulting from uncertainties in the soil uptake lifetime. As with $CH_4$, we also determine a level of self-feedback on the chemical lifetime for $H_2$ in our model simulations. However, this has a negligible impact on the total $H_2$ lifetime due to the dominance of the soil sink.

**Table 9: The range of hydrogen soil deposition lifetimes from existing literature studies and the resulting total hydrogen lifetime when combined with the chemical lifetime of 8.3 years from UKESM1. The $H_2$ budget studies included in the calculation of the mean are: Novelli et al., 1999; Yashiro et al., 2001; Hauglustaine and Ehhalt, 2002; Sanderson et al., 2003; Rhee et al., 2006; Xiao et al., 2007; Price et al., 2007; Ehhalt and Rohrer, 2009; Pieterse et al., 2013; Paulot et al., 2021.**

| $\tau_{H2SOIL}$ (years) | $\alpha_H$ (years) |
|---|---|
| 1.7 (min) | 1.4 |
| 2.5 (mean) | 1.9 |
| 2.9 (max) | 2.2 |

## 6.4 A Global Warming Potential for hydrogen

A total GWP for $H_2$ can be obtained by summing the GWPs resulting from perturbations to $CH_4$, tropospheric ozone and stratospheric water vapour following an increase in $H_2$. The calculations of the $H_2$ GWPs for each of these radiatively active species are outlined in Annex 1 and are based on chemical composition changes and time constants derived from our UKESM simulations, along with radiative efficiency scaling factors from IPCC (2014, 2021). We do not use the effective radiative forcings determined from UKESM1 (see Section 5) in the GWP calculations as the calculated ERFs cannot be attributed to changes in individual chemical species, which will vary with different time constants following a pulse emission (required for calculating GWPs from steady-state simulations). Changes to stratospheric ozone are not included in our GWP calculations as, based on results from our UKESM1 simulations (see Annex 1), we determine its contribution to the time integrated radiative forcing to be negligible. Using radiative efficiencies and the absolute global warming potential (AGWP) for $CO_2$ from IPCC AR5 (IPCC, 2014), we obtain a total GWP(100) for $H_2$ of $11 \pm 5$, accounting for uncertainties in the hydrogen soil sink, radiative forcing scaling factors and the AGWP for $CO_2$ (see Table 10). For a 20 year time horizon, we obtain a GWP(20) for $H_2$ of 33, with an uncertainty range of 20 to 44.

We find that using updated radiative forcing scaling factors from IPCC (2021) slightly increases the indirect $H_2$ GWP due to $CH_4$, whilst decreasing the indirect GWPs resulting from tropospheric ozone and stratospheric water vapour, relative to IPCC (2014) (see Table 11). These effects approximately cancel and the difference in total $H_2$ GWPs based on IPCC (2014) and IPCC (2021) data is negligible relative to our uncertainties.

The only previous studies to estimate a GWP(100) for $H_2$, Derwent et al. (2020) (hereafter referred to as D2020) and Field and Derwent (2021) (hereafter referred to as FD2021) obtained values of $5 \pm 1$ and $3.3 \pm 1.4$ respectively, based on changes to the troposphere only. Our value of $11 \pm 5$ therefore represents a significant increase in the $H_2$ GWP(100) relative to

previous estimates. In part this is due to the inclusion of the stratosphere in our study, which accounts for approximately 30% of the GWP. Excluding the stratosphere, our troposphere-only GWP(100) of 7.9 (4.3 to 11.5) is still larger than the previous estimates, although there is some overlap within the uncertainty bounds.

Part of the difference between the troposphere-only $H_2$ GWP(100)s in this study and that of D2020 and FD2021 likely arises from the different methods employed to determine the $H_2$ GWP. Whereas we derive an $H_2$ GWP from steady-state model simulations, both D2020 and FD2021 use transient simulations that were however run for only a limited period (5 years in the case of D2020, 60 years in the case of FD2021), and then extrapolated to 100 years to determine a GWP(100). The time constants used in the extrapolation were based on e-folding decay time constants for the $CH_4$ perturbation lifetime (for $CH_4$) and the $H_2$ lifetime (for $O_3$). In the case of the 5 year simulation by D2020, this method will result in an underestimate of the $H_2$ GWP(100), as the assumption that $CH_4$ will simply decay according to a time constant of the $CH_4$ perturbation lifetime after 5 years neglects the influence of any $H_2$ from the pulse remaining in the atmosphere that will continue to perturb the atmospheric composition, and $CH_4$ in particular. In addition, assuming that the $O_3$ perturbation will decay according to a time constant of the $H_2$ lifetime between 5 and 100 years after the pulse neglects a longer-scale time constant associated with the influence of $CH_4$ on ozone that will also result in an underestimate of the $H_2$ GWP. Due to these reasons, we would expect our value for the $H_2$ GWP(100) to be larger than that derived by D2020. As the model simulation in FD2021 was run for 60 years before extrapolating, we would expect these decay rate assumptions to have less of an impact on their $H_2$ GWP(100) value. Part of the difference between the $H_2$ GWPs in this study and FD2021 can be attributed to FD2021 using a radiative forcing scaling factor for changes in ozone that is approximately 25% lower than the value applied in this study (Stevenson et al., 2013), although this is likely to have a relatively minor effect (resulting in a difference in the $H_2$ GWP of less than 1).

A recent study by Paulot et al. (2021) estimated the indirect radiative forcing at steady-state due to an increase in $H_2$ emissions using the GFDL-AM4.1 chemistry-climate model, but did not calculate a GWP for $H_2$. Paulot et al. (2021) found that $H_2$ causes an indirect forcing of 0.13 mW $m^{-2}$ ppb$(H_2)^{-1}$. We obtain a value of 0.18 $\pm$ 0.03 mW $m^{-2}$ ppb$(H_2)^{-1}$ based on the steady-state changes in composition in our UKESM1 TS2014_2000$H_2$ and TS2014_2000$H_2$_2171$CH_4$ simulations and the IPCC (2014) radiative forcing scaling factors with the uncertainties as outlined above. The difference between our calculated radiative forcing per ppb $H_2$ and that of Paulot et al. (2021) can be attributed to larger radiative forcings for both $CH_4$ and tropospheric ozone per ppb $H_2$ derived in our study. As the majority of the ozone forcing (~66%) in this study is methane-induced, part of the difference in the $CH_4$ and ozone radiative forcings between this study and Paulot et al. (2021) can be explained by the larger $CH_4$ feedback factor in UKESM1 (1.49) relative to the chemistry-climate model used in Paulot et al. (2021) (1.3). This will lead to a larger change in $CH_4$ for a fixed change in $H_2$ in UKESM1 relative to Paulot et al. (2021). The $CH_4$ feedback factor of 1.49 derived here for UKESM1 is at the top of a range of values of 1.19 to 1.43 for six different models (Thornhill et al. 2021), and as such may lead to a larger $H_2$ GWP relative to a model with a mid-range feedback factor. However, uncertainties in the GWP due to the $CH_4$ feedback factor are likely to be relatively minor when

compared with uncertainties due to the hydrogen soil sink. The radiative forcing per ppb $H_2$ obtained for stratospheric water vapour is identical in our study and that of Paulot et al. (2021), as is the conclusion that the radiative forcing resulting from changes in stratospheric ozone is negligible.

**Table 10: Indirect radiative forcings arising from a change in the $H_2$ LBC based on changes in composition in our UKESM1 and box model simulations, along with the associated GWP(100)s for $H_2$ calculated using equations E1 to E4.**

| Radiatively active species | Radiative Forcing at steady-state (mW $m^{-2}$ $ppbH_2^{-1}$) | $H_2$ GWP (100) | GWP range – soil sink uncertainties | Uncertainty arising from RF scaling factors and $AGWP_{CO2}$ | Total GWP(100) range |
|---|---|---|---|---|---|
| Methane | 0.08 | 4.7 | 3.5 – 5.5 | ± 28% | 2.5 – 7.0 |
| Tropospheric ozone (methane and non-methane induced) | 0.06 | 3.2 | 2.3 – 3.7 | ± 47% | 1.2 – 5.5 |
| **Total Troposphere** | **0.14** | **7.9** | **5.7 – 9.2** | **± 25%** | **4.3 – 11.5** |
| Stratospheric water vapour (methane and non-methane induced) | 0.04 | 3.0 | 2.2 – 3.5 | ± 31% | 1.5 – 4.8 |
| **Total** | **0.18 ± 0.03** | **10.9** | **7.9 – 12.7** | **± 20%** | **6.4 – 15.3** |

**Table 11: A comparison of the 100 and 20 year time horizon $H_2$ GWPs (GWP(100) and GWP(20) respectively) determined using radiative efficiencies and the AGWP for $CO_2$ from IPCC AR5 (2014) and from IPCC AR6 (2021).**

| Radiatively active species | $H_2$ GWP(100) IPCC AR5 | $H_2$ GWP(100) IPCC AR6 | $H_2$ GWP(20) IPCC AR5 | $H_2$, GWP(20) IPCC AR6 |
|---|---|---|---|---|
| Methane | 4.7 | 5.2 | 13.3 | 14.6 |
| Tropospheric ozone (methane and non-methane induced) | 3.2 | 2.7 | 9.6 | 8.4 |
| **Total Troposphere** | **7.9** | **7.9** | **22.9** | **23.0** |
| Stratospheric water vapour (methane and non-methane induced) | 3.0 | 2.9 | 9.6 | 9.2 |
| **Total** | **10.9 (6.4 – 15.3)** | **10.8** | **32.6 (19.7 – 44.1)** | **32.2** |

## 6.5 Net climate impact of the disbenefits arising from Hydrogen leakage and expected Carbon Dioxide emission reductions

Any leakage of $H_2$ will result in an indirect global warming, offsetting greenhouse gas emission reductions made as a result of a switch from fossil fuel to $H_2$. Determining a GWP for $H_2$ allows a change in $H_2$ emissions to be compared to an equivalent change in carbon dioxide emissions in terms of time integrated radiative forcing. This increase in equivalent carbon dioxide emissions can be compared with expected reductions in carbon dioxide and $CH_4$ (as equivalent $CO_2$) emissions to determine the net impact on radiative forcing.

In our illustrative future global hydrogen economy scenario, described in Section 3.1, we estimate additional $H_2$ emissions of between 9 and 95 Tg $yr^{-1}$. Using a $H_2$ GWP(100) of 11, this is equivalent to the time integrated radiative forcing from carbon dioxide emissions of about 100 and 1050 Tg $CO_2$ $yr^{-1}$ respectively. Based on the fossil fuel energy sectors that are replaced by $H_2$ (see Section 3.1), a low carbon method of hydrogen generation and the sector emissions described in Hoesly et al. (2018), we would expect a reduction in carbon dioxide emissions of ~26,000 Tg $yr^{-1}$ (see Table 5). In addition a further reduction of ~1200 Tg $yr^{-1}$ equivalent $CO_2$ emissions would result from expected $CH_4$ emission reductions (assuming a GWP(100) for $CH_4$ of 28 and the $CH_4$ emission reductions outlined in Table 2), resulting in a total reduction of $CO_2$ equivalent emissions of ~27,200 Tg $yr^{-1}$. Therefore, in this global scenario the increase in equivalent $CO_2$ emissions based on 1% and 10% $H_2$ leakage rate offsets approximately 0.4 and 4% of the total equivalent $CO_2$ emission reductions respectively.

Whilst the benefits from equivalent $CO_2$ emission reductions significantly outweigh the disbenefits arising from $H_2$ leakage, they clearly demonstrate the importance of controlling $H_2$ leakage within a hydrogen economy.

## 6.6 Hydrogen GWP Uncertainties

The uncertainty range in the $H_2$ GWPs quoted above includes uncertainties associated with the magnitude of the $H_2$ soil sink, radiative forcing scaling factors and the AGWP for carbon dioxide. It does not account for uncertainties in the chemical lifetime of $H_2$, e-folding lifetimes of the chemical perturbations, the $CH_4$ feedback factor or the production rate of radiatively active species per unit change in $H_2$ mixing ratio ('a', see Annex 1). These values are derived from our UKESM1 simulations and are likely to vary when using different atmospheric models with different chemistry schemes. As these parameters contain correlated uncertainties, further simulations using different models and different chemistry schemes would be required to fully assess the impact of uncertainties in these parameters on the $H_2$ GWP. In addition, we also note that the sensitivity of ERF in UKESM to changes in $CH_4$ is significantly larger (approximately double) that indicated by the radiative scaling factors used in the empirical relationships applied in the GWP calculation. This suggests a further source of uncertainty, associated with the response of aerosols and clouds to changing $CH_4$ levels (see Section 5.3), than accounted for by the radiative forcing scaling factor uncertainties outlined in IPCC (2014) and Annex 1.

The largest source of uncertainty in the $H_2$ GWP in this study is due to uncertainties in the soil deposition lifetime of $H_2$. For a short soil deposition lifetime, a greater fraction of additional $H_2$ emissions from a hydrogen economy will be deposited to the soil, leaving less to react with atmospheric OH and induce chemical feedbacks, and vice versa for a long soil deposition lifetime. Reducing the uncertainty of the GWP for $H_2$ and its other atmospheric impacts could therefore be best achieved by an improved understanding of the hydrogen soil sink, and how it may change under future climate scenarios and higher atmospheric $H_2$ concentrations.

The model configuration used in this study employed fixed lower boundary conditions for $H_2$ and $CH_4$. A box model was used to define these boundary conditions under changing emissions and allowing for chemical feedbacks in the system. This approach has been widely used previously to study the climate impact of changes in $CH_4$. However, in this case interactions between composition and surface processes are subsumed into the lower boundary condition. An alternative approach would be to replace the use of fixed lower boundary concentrations by specified or modelled emission fluxes into the atmosphere. In the case of $H_2$, the surface deposition could then be modelled explicitly, depending on the underlying surface. Different treatments of deposition, its process, magnitude and dependence on climate parameters, which have been highlighted here as an important source of uncertainty, could then be explored and the impact of regional changes in emissions of $H_2$, $CH_4$ or the co-emitted species, could be meaningfully assessed. Changing emissions using the flux based approach would also allow a direct evaluation of the GWP. Finally, model sensitivity to emissions or changes in the lower boundary conditions will depend to some extent on the background state reproduced by the model. Future studies should explore that sensitivity.

# 7 Conclusions

Using hydrogen ($H_2$) as an energy source is an important plank in the strategy to avoid fossil fuel emissions. If hydrogen is produced cleanly, it offers a major climate advantage not just because of the reduction in carbon dioxide ($CO_2$) and methane ($CH_4$) emissions, two major greenhouse gases, but also because of the opportunity to reduce other emissions including those of carbon monoxide (CO), volatile organic compounds (VOCs) and oxides of nitrogen ($NO_x$), which would produce an additional air quality benefit. (We note that, in some sectors where hydrogen is combusted, $NO_x$ emissions could increase with negative consequences for air quality; we have not considered $NO_x$ increases here.) Leakage of hydrogen into the atmosphere would have a wider impact on atmospheric composition, which will partially offset some of the gains obtained in a switch to hydrogen. Similarly, the net-benefit will also depend on the extent to which other emissions are reduced.

In this study we have focussed on the consequences of hydrogen leakage. We have used a state-of-the-art chemistry-climate model, UKESM1, to calculate changes in atmospheric composition, which might follow that leakage into the atmosphere. We have considered a range of cases for increases in the atmospheric hydrogen abundance as well as cases where emissions of other gases are reduced. The impact of these changes on radiative forcing have also been considered.

The benefit of any switch to a hydrogen-based economy depends on the extent to which a range of technologies are switched away from the use of fossil fuel and the associated reductions in carbon dioxide emissions. We have not attempted to model the potentially large benefit of the carbon dioxide reduction. Our focus has been the exploration of the impacts on composition and climate of the other changes mentioned above.

In a final part of our study, we have evaluated the global warming potential (GWP) of hydrogen. Hydrogen is not a greenhouse gas but changes in its atmospheric abundance will change the concentrations of the important greenhouse gases methane, water vapour, and ozone, both in the troposphere and stratosphere. We have used modelled changes to these gases in response to changing atmospheric hydrogen mixing ratios to produce the most comprehensive assessment to date of the hydrogen GWP.

**Atmospheric Composition**

We developed a number of scenarios to explore the atmospheric response to changes in the emissions of hydrogen and other species associated with a shift to a hydrogen economy. The extent of any change depends on the uptake of hydrogen and the fossil fuel technologies replaced. It also depends on the leakage of hydrogen in the supply chain. These things are uncertain, and so we have explored a range of potential changes to the atmospheric hydrogen burden. We have endeavoured to model the impact of large but plausible changes, allowing us to both detect a signal of change and to explore the linearity of these changes over a range of atmospheric hydrogen mixing ratios. To this end, we have modelled the impact of increases in hydrogen from its current background concentration of about 0.5 ppm to values up to 2 ppm;

values which we believe span much of the uncertainty range of any future hydrogen economy as well previous literature estimates (e.g. Tromp et al., 2003; Warwick et al. 2004; Schultz et al. 2003).

Hydrogen leakage will affect the concentration of methane, ozone and water vapour in the atmosphere. The changes in methane and ozone are driven by changes in the hydroxyl radical, OH, which is the major atmospheric oxidant and a key player in the chemistry of the atmosphere. hydrogen acts as a chemical sink for OH, and so increases in hydrogen concentrations lead to a reduction in tropospheric OH, which in turn results in an increase to the methane lifetime. Based on our experiments we conclude that if methane emissions remain constant, increased hydrogen emissions would result in a longer methane lifetime and a higher methane abundance. In calculations driven only by a change in hydrogen, the methane lifetime increases linearly with the hydrogen increase. When the hydroxyl radical feedback on methane abundance is included, for every 1 ppm increase in hydrogen, the methane lifetime increases by about a year, and methane increases by about 12% (from 1835 ppb in TS2014_BASE to 2058 ppb in TS_2014_1500$H_2$_2058$CH_4$), if methane emissions remain constant. When reductions in emissions of carbon monoxide, oxides of nitrogen and volatile organic compounds are also considered alongside increases to atmospheric hydrogen, the decrease in hydroxyl radical, and hence increase in methane, is smaller. The response of methane to a shift to an hydrogen economy is complex and strongly scenario dependent. Our range of scenarios covers both possible increases and decreases in methane. Under the maximum increase of 1.5 ppm of hydrogen considered here, to offset the potential increase in methane would require further decreases in not just emissions of methane, but also the co-emitted species of carbon monoxide, oxides of nitrogen and volatile organic compounds.

The response of tropospheric ozone is equally complex and depends not simply on the changes in hydrogen abundance but also on changes in the emissions of other species as the ozone abundance is controlled by a series of complex production and loss cycles in which hydroxyl radicals, methane, other volatile organic compounds and oxides of nitrogen all play a role. For the scenarios considered here, an increase in atmospheric hydrogen only results in a small increase in tropospheric ozone (~1.3% per ppm of hydrogen). If methane increases which will result from increased atmospheric hydrogen are also considered, larger increases in ozone are modelled. Only scenarios which model decreases in the emission of carbon monoxide, oxides of nitrogen and volatile organic compounds produce decreases in tropospheric ozone. A linear relationship has been identified between the change in atmospheric hydrogen and tropospheric ozone, allowing an estimate of the ozone response to a given change in atmospheric hydrogen even if that specific scenario has not been considered in this study. However, the gradient of this relationship is strongly dependent on the emissions of carbon monoxide, oxides of nitrogen, volatile organic compounds and methane associated with the shift to a hydrogen economy. In scenarios which assume reductions in the emissions of carbon monoxide, oxides of nitrogen, and volatile organic compounds, tropospheric ozone can decrease despite increases to atmospheric hydrogen and methane, which is a positive for air quality mitigation efforts. However, in these scenarios the ozone change is spatially heterogeneous.

`Atmospheric implications of increased hydrogen use

Stratospheric ozone is controlled by different chemical processes to those in the troposphere. The increased flux of hydrogen to the stratosphere leads to increases in water vapour. (Note that we have not considered direct production of water vapour in the stratosphere from possible future hydrogen-fuelled aviation.) Methane also increases in parts of the stratosphere and together these changes lead to an increased production of hydroxyl radicals there and, through much of the stratosphere, ozone decreases. These changes are small in the lower to middle stratosphere, where the bulk of stratospheric ozone is found, with larger decreases in the upper stratosphere, driven by the increase in hydroxyl radicals, and, to some extent, in polar latitudes, where increased water vapour plays a role. For the range of calculations performed, we find no discernible negative impacts on global stratospheric ozone recovery of adoption of a global hydrogen economy.

**Radiative forcing**

Adoption of hydrogen as an energy source could save large emissions of carbon dioxide and provide a significant climate benefit but any increases in tropospheric ozone, water vapour and methane, consequent on increases in atmospheric hydrogen would all tend to increase radiative forcing, partially offsetting the climate benefits of a switch to hydrogen. We have assessed this, first, by considering the change in radiative forcing calculated in the various scenarios that we considered. Second, we have made a new determination of hydrogen's GWP.

The net top-of-atmosphere radiative forcing change depends strongly on the hydrogen leakage rate, on any associated reduction in methane emissions and on the extent of co-emission benefits. In calculations where we assume leakage of hydrogen into the atmosphere, our calculations indicate an increase in radiative forcing (i.e., a warming tendency).

When only hydrogen increases in our model experiments, we calculate an effective radiative forcing of 0.148 W $m^{-2}$ for an increase in hydrogen of 1.5 ppm; when the methane lower boundary is increased by 340 ppb, consistent with the hydrogen-induced decrease in hydroxyl radicals, the radiative forcing approaches 0.5 W $m^{-2}$. In contrast, if there is no leakage of hydrogen into the atmosphere, and methane and other co-emissions are reduced, the radiative forcing is -0.29 W $m^{-2}$ (a cooling tendency). Assuming a climate sensitivity of 0.86 K $W^{-1}$ $m^2$, this level of radiative forcing if sustained would lead to equilibrium global-mean temperature changes of 0.12, 0.43 and -0.26 ˚C without accounting for the reduced emissions of carbon dioxide that would result.

The net top-of-atmosphere radiative forcing varies strongly regionally. It depends in a complex fashion on the changes in gas phase composition, the subsequent impact on aerosol production and on cloud and aerosol interactions. Further studies would be required to explore regional impacts in more detail.

The changes in radiative forcing, like the changes in atmospheric composition, indicate that, to maximize the climate and air quality benefit of a transition to a hydrogen-powered economy, minimisation of both hydrogen leakage and a reduction of the ancillary emissions of, for example, CO, $NO_x$ and VOCs is required.

`Atmospheric implications of increased hydrogen use

**Global warming potential**

GWPs have been calculated previously for short-lived species (e.g. $NO_x$ from aviation) whose emissions result in indirect radiative forcings. However, the methodology used previously is not appropriate for gases with intermediate and longer lifetimes such as hydrogen, with a lifetime of several years. We have developed a modified approach which now considers the lifetime of the pulse gas ($H_2$) in addition to the lifetimes of the radiatively active gases causing the indirect forcing (ozone, methane and water vapour), allowing the GWP of hydrogen to be evaluated. While hydrogen-induced changes in methane and ozone in the troposphere have been considered previously, we have also considered, for the first time, previously ignored changes in stratospheric water vapour and stratospheric ozone in our calculations of hydrogen's GWP.

We estimate the hydrogen GWP(100) to be $11 \pm 5$; a value more than 100% larger than previously published calculations. About a third of this arises from the changes in stratospheric water vapour that follow from an increase in atmospheric hydrogen.

The majority of uncertainty in the GWP arises from uncertainty with regard to the natural budget of atmospheric hydrogen, where the magnitude of the soil sink for hydrogen is the most uncertain factor. Future work is required to resolve these atmospheric uncertainties.

While the model used for this study includes a comprehensive chemistry scheme, for both hydrogen and methane we employed specified lower boundary surface concentrations. Future model calculations should complement our work with transient experiments using flux boundary conditions.

# 8 References

Alvarez, R.A., Zavala-Araiza, D., Lyon, D.R., Allen, D.T., Barkley, Z.R., Brandt, A.R., Davis, K.J., Herndon, S.C., Jacob, D.J., Karion, A. and Kort, E.A., 2018. Assessment of methane emissions from the US oil and gas supply chain. Science, 361(6398), pp.186-188.

Archibald, A. T., O'Connor, F. M., Abraham, N. L., Archer-Nicholls, S., Chipperfield, M. P., Dalvi, M., Folberth, G. A., Dennison, F., Dhomse, S. S., Griffiths, P. T., Hardacre, C., Hewitt, A. J., Hill, R. S., Johnson, C. E., Keeble, J., Köhler, M. O., Morgenstern, O., Mulcahy, J. P., Ordóñez, C., Pope, R. J., Rumbold, S. T., Russo, M. R., Savage, N. H., Sellar, A., Stringer, M., Turnock, S. T., Wild, O., and Zeng, G.: Description and evaluation of the UKCA stratosphere–troposphere chemistry scheme (StratTrop vn 1.0) implemented in UKESM1, Geosci. Model Dev., 13, 1223–1266, https://doi.org/10.5194/gmd-13-1223-2020, 2020.

BP Energy Outlook, Energy Economics, https://www.bp.com/en/global/corporate/energy-economics.html, 2020.

Collins, W. J., Lamarque, J.-F., Schulz, M., Boucher, O., Eyring, V., Hegglin, M. I., Maycock, A., Myhre, G., Prather, M., Shindell, D., and Smith, S. J.: AerChemMIP: quantifying the effects of chemistry and aerosols in CMIP6, Geosci. Model Dev., 10, 585–607, https://doi.org/10.5194/gmd-10-585-2017, 2017.

Derwent, R., Simmonds, P., O'Doherty, S., Manning, A., Collins, W. and Stevenson, D.: Global environmental impacts of the hydrogen economy, International Journal of Nuclear Hydrogen Production and Applications, 1(1), 57-67, 2006.

Derwent, R.G., Stevenson, D.S., Utembe, S.R., Jenkin, M.E., Khan, A.H. and Shallcross, D.E.: Global modelling studies of hydrogen and its isotopomers using STOCHEM-CRI: Likely radiative forcing consequences of a future hydrogen economy, International Journal of Hydrogen Energy, 45(15), 9211-9221, 2020.

Duncan, B. N, Logan, J. A., Bey, I., Megretskaia, I. A., Yantosca, R. M., Novelli, P. C., Jones, N. B., and Rinsland, C. P.: Global budget of CO, 1988–1997: Source estimates and validation with a global model, J. Geophys. Res. 112, D22301, doi:10.1029/2007JD008459, 2007.

E4tech, Ltd: $H_2$ emission potential review, BEIS Research Paper Number 22, 2019.

Ehhalt, D. H. and Rohrer, F.: The tropospheric cycle of $H_2$: a critical review, Tellus B, 61, 500–535, 2009.

Field, R.A. and Derwent, R., Global warming consequences of replacing natural gas with hydrogen in the domestic energy sectors of future low-carbon economies in the United Kingdom and the United States of America, International Journal of Hydrogen Energy, 46, 30,190-30,203, 2021.

`Atmospheric implications of increased hydrogen use

Fuglestvedt, J. S., Shine, K. P., Berntsen, T., Cook, J., Lee, D. S., Stenke, A., Skeie, R. B., Velders, G. J. M., and Waitz, I. A.: Transport impacts on atmosphere and climate: Metrics, Atmos. Environ., 44, 4648–4677, 2010.

Galanter, M., Levy II, H., and Carmichael, G. R.: Impacts of biomass burning on tropospheric CO, $NO_x$, and $O_3$, J. Geophys. Res., 105, 6633–6653, 2000.

Gidden, M. J., Riahi, K., Smith, S. J., Fujimori, S., Luderer, G., Kriegler, E., van Vuuren, D. P., van den Berg, M., Feng, L., Klein, D., Calvin, K., Doelman, J. C., Frank, S., Fricko, O., Harmsen, M., Hasegawa, T., Havlik, P., Hilaire, J., Hoesly, R., Horing, J., Popp, A., Stehfest, E., and Takahashi, K.: Global emissions pathways under different socioeconomic scenarios for use in CMIP6: a dataset of harmonized emissions trajectories through the end of the century, Geosci. Model Dev., 12, 1443–1475, https://doi.org/10.5194/gmd-12-1443-2019, 2019.

Hauglustaine, D. A. and Ehhalt, D. H.: A three-dimensional model of molecular hydrogen in the troposphere, J. Geophys. Res., 107(D17), 4330, doi:10.1029/2001JD001156, 2002.

Heimann, I., Griffiths, P. T., Warwick, N. J., Abraham, N. L., Archibald, A. T., & Pyle, J. A.: Methane emissions in a chemistry-climate model: Feedbacks and climate response, J. Adv. Model. Earth Sy, 12, e2019MS002019, https://doi.org/10.1029/2019MS002019, 2020.

Hoesly, R. M., Smith, S. J., Feng, L., Klimont, Z., Janssens-Maenhout, G., Pitkanen, T., Seibert, J. J., Vu, L., Andres, R. J., Bolt, R. M., Bond, T. C., Dawidowski, L., Kholod, N., Kurokawa, J.-I., Li, M., Liu, L., Lu, Z., Moura, M. C. P., O'Rourke, P. R., and Zhang, Q.: Historical (1750–2014) anthropogenic emissions of reactive gases and aerosols from the Community Emissions Data System (CEDS), Geosci. Model Dev., 11, 369–408, https://doi.org/10.5194/gmd-11-369-2018, 2018.

IPCC: Climate Change 2014: Synthesis Report. Contribution of Working Group I to the Fifth Assessment Report of the Intergovernmental Panel on Climate Change [Core Writing Team, R.K. Pachauri and L.A. Meyer (eds.)]. IPCC, Geneva, Switzerland, 151 pp, 2014.

IPCC: Climate Change 2021: The Physical Science Basis. Contribution of Working Group I to the Sixth Assessment Report of the Intergovernmental Panel on Climate Change, edited by: Masson-Delmotte, V., Zhai, P., Pirani, A., Connors, S.L., Péan, C., Berger, S., Caud, N., Chen, Y., Goldfarb, L., Gomis, M.I., Huang, M., Leitzell, K., Lonnoy, E., Matthews, J.B.R., Maycock, T.K., Waterfield, T., Yelekçi, O., Yu, R., and Zhou, B., Cambridge University Press, 2021.

Myhre, G., Nilsen, J. S., Gulstad, L., Shine, K. P., Rognerud, B., and Isaksen, I. S. A.: Radiative forcing due to stratospheric water vapour from $CH_4$ oxidation, Geophys. Res. Lett., 34, L01807, https://doi.org/10.1029/2006GL027472, 2007.

Myhre, G. Highwood, E.J., Shine, K.P., Stordal, F., New estimates of radiative forcing due to well mixed greenhouse gases, Geophys. Res. Lett. 25, 14, https://doi.org/10.1029/98GL01908, 1998.

Nisbet, E., Fisher, R., Lowry, D., France, J., Allen, G., Bakkaloglu, S., Broderick, T., Cain, M., Coleman, M., Fernandez, J., Forster, G., Griffiths, P., Iverach, C., Kelly, B., Manning, M., Nisbet-Jones, P., Pyle, J., Townsend-Small, A., Al-Shalaan, A., Warwick, N., and Zazzeri, G.: Methane mitigation: methods to reduce emissions, on the path to the Paris Agreement, Rev. Geophys., 58, e2019RG000675, https://doi.org/10.1029/2019rg000675, 2020.

Novelli, P. C., Lang, P. M., Masarie, K. A., Hurst, D. F., Myers, R., and Elkins, J. W.: Molecular hydrogen in the troposphere: Global distribution and budget, J. Geophys. Res., 104(D23), 30 427–30 444, 1999.

O'Connor, F.M., Abraham, N.L., Dalvi, M., Folberth, G.A., Griffiths, P.T., Hardacre, C., Johnson, B.T. ,Kahana, R., Keeble, J., Kim, B., Morgenstern, O., Mulcahy, J.P., Richardson, M., Robertson, E., Seo, J., Shim, S., Teixeira, J.C., Turnock, S.T., Williams, J., Wiltshire, A.J., Woodward, S., and Zeng, G., Assessment of pre-industrial to present-day anthropogenic climate forcing in UKESM1, Atmospheric Chemistry and Physics, 21, 1211–1243, 2021.

Paulot, F., Paynter, D., Naik, V., Malyshev, S., Menzel, R. and Horowitz, L.W.: Global modeling of hydrogen using GFDL-AM4. 1: Sensitivity of soil removal and radiative forcing, International Journal of Hydrogen Energy, 46(24), 13446-13460, 2021.

Pieterse, G., Krol, M. C., Batenburg, A. M., Brenninkmeijer, C. A. M., Popa, M. E., O'Doherty, S., Grant, A., Steele, L.P., Krummel, P. B., Langenfelds, R.L., Wang, H. J., Vermeulen, A. T., Schmidt, M., Yver, C., Jordan, A., Engel, A., Fisher, R. E., Lowry, D., Nisbet, E. G., Reimann, S., Vollmer, M. K., Steinbacher, M., Hammer, S., Forster, G., Sturges, W. T., and Röckmann, T.: Reassessing the variability in atmospheric $H_2$ using the two-way nested TM5 model, J. Geophys. Res.-Atmos., 118, 3764–3780, doi:10.1002/jgrd.50204, 2013.

Prather, M.J.: Lifetimes and eigenstates in atmospheric chemistry, Geophysical Research Letters, 21(9), 801-804, 1994.

Prather, M. J., Holmes, C. D., and Hsu, J.: Reactive greenhouse gas scenarios: Systematic exploration of uncertainties and the role of atmospheric chemistry, Geophys. Res. Lett., 39, L09803, https://doi.org/10.1029/2012GL051440, 2012.

Price, H., Jaeglé, L., Rice, A., Quay, P., Novelli, P.C. and Gammon, R.: Global budget of molecular hydrogen and its deuterium content: Constraints from ground station, cruise, and aircraft observations, Journal of Geophysical Research: Atmospheres, 112(D22), 2007.

Rhee, T. S., Brenninkmeijer, C. A. M., and Röckmann, T.: The overwhelming role of soils in the global atmospheric hydrogen cycle, Atmos. Chem. Phys., 6, 1611–1625, https://doi.org/10.5194/acp-6-1611-2006, 2006.

Sanderson, M. G., Collins, W. J., Derwent, R. G., and Johnson, C. E.: Simulation of global hydrogen levels using a Lagrangian three-dimensional model, J. Atmos. Chem., 46, 15–28, 2003.

`Atmospheric implications of increased hydrogen use

Saunois, M., Stavert, A. R., Poulter, B., Bousquet, P., Canadell, J. G., Jackson, R. B., Raymond, P. A., Dlugokencky, E. J., Houweling, S., Patra, P. K., Ciais, P., Arora, V. K., Bastviken, D., Bergamaschi, P., Blake, D. R., Brailsford, G., Bruhwiler, L., Carlson, K. M., Carrol, M., Castaldi, S., Chandra, N., Crevoisier, C., Crill, P. M., Covey, K., Curry, C. L., Etiope, G., Frankenberg, C., Gedney, N., Hegglin, M. I., Höglund-Isaksson, L., Hugelius, G., Ishizawa, M., Ito, A., Janssens-Maenhout, G., Jensen, K. M., Joos, F., Kleinen, T., Krummel, P. B., Langenfelds, R. L., Laruelle, G. G., Liu, L., Machida, T., Maksyutov, S., McDonald, K. C., McNorton, J., Miller, P. A., Melton, J. R., Morino, I., Müller, J., Murguia-Flores, F., Naik, V., Niwa, Y., Noce, S., O'Doherty, S., Parker, R. J., Peng, C., Peng, S., Peters, G. P., Prigent, C., Prinn, R., Ramonet, M., Regnier, P., Riley, W. J., Rosentreter, J. A., Segers, A., Simpson, I. J.,

Shi, H., Smith, S. J., Steele, L. P., Thornton, B. F., Tian, H., Tohjima, Y., Tubiello, F. N., Tsuruta, A., Viovy, N., Voulgarakis, A., Weber, T. S., van Weele, M., van der Werf, G. R., Weiss, R. F., Worthy, D., Wunch, D., Yin, Y., Yoshida, Y., Zhang, W., Zhang, Z., Zhao, Y., Zheng, B., Zhu, Q., Zhu, Q., and Zhuang, Q.: The Global Methane Budget 2000–2017, Earth Syst. Sci. Data, 12, 1561–1623, https://doi.org/10.5194/essd-12-1561-2020, 2020.

Schultz, M., Diehl, T., Brasseur, G. P. and Zittel, W., Air pollution and climate-forcing impacts of a global hydrogen economy, Science, 302, 624-627, 2003.

Schwarzkopf, M. D. and Ramaswamy, Radiative forcing due to ozone in the 1980s: dependence on altitude of ozone change, Geophys. Res. Lett., 20, 205-208, 1993.

Sellar, A. A., Jones, C. G., Mulcahy, J., Tang, Y., Yool, A., Wiltshire, A., O'Connor, F. M., Stringer, M., Hill, R., Palmieri, J., Woodward, S., de Mora, L., Kuhlbrodt, T., Rumbold, S., Kelley, D. I., Ellis, R., Johnson, C. E., Walton, J., Abraham, N. L., Andrews, M. B., Andrews, T., Archibald, A. T., Berthou, S., Burke, E., Blockley, E., Carslaw, K., Dalvi, M., Edwards, J., Folberth, G. A., Gedney, N., Griffiths, P. T., Harper, A. B., Hendry, M. A., Hewitt, A. J., Johnson, B., Jones, A., Jones, C. D., Keeble, J., Liddicoat, S., Morgenstern, O., Parker, R. J., Predoi, V., Robertson, E., Siahaan, A., Smith, R. S., Swaminathan, R., Woodhouse, M. T., Zeng, G., and Zerroukat, M.: UKESM1: Description and evaluation of the UK Earth System Model, J. Adv. Model. Earth Sy., 11, 4513–4558, https://doi.org/10.1029/2019ms001739, 2020.

Smith-Downey, N. V., Randerson, J. T., and Eiler, J. M.: Molecular hydrogen uptake in forest, desert, and marsh ecosystems in California, J. Geophys. Res., 113, G03037, doi:10.1029/2008JG000701, 2008.

Staffell, I., Scamman, D., Abad, A.V., Balcombe, P., Dodds, P.E., Ekins, P., Shah, N. and Ward, K.R.: The role of hydrogen and fuel cells in the global energy system, Energy & Environmental Science, 12(2), 463-491, 2019.

Stevenson, D. S., Young, P. J., Naik, V., Lamarque, J.-F., Shindell, D. T., Voulgarakis, A., Skeie, R. B., Dalsoren, S. B., Myhre, G., Berntsen, T. K., Folberth, G. A., Rumbold, S. T., Collins, W. J., MacKenzie, I. A., Doherty, R. M., Zeng, G., van Noije, T. P. C., Strunk, A., Bergmann, D., Cameron-Smith, P., Plummer, D. A., Strode, S. A., Horowitz , L., Lee, Y. H., Szopa, S., Sudo, K., Nagashima , T., Josse, B., Cionni, I., Righi, M., Eyring, V., Conley, A.,

`Atmospheric implications of increased hydrogen use

Bowman, K. W., Wild, O., and Archibald, A.: Tropospheric ozone changes, radiative forcing and attribution to emissions in the Atmospheric Chemistry and Climate Model Intercomparison Project (ACCMIP), Atmos. Chem. Phys., 13, 3063–3085, https://doi.org/10.5194/acp-13-3063-2013, 2013.

Thornhill, G. D., Collins, W. J., Kramer, R. J., Olivié, D., Skeie, R. B., O'Connor, F. M., Abraham, N. L., Checa-Garcia, R., Bauer, S. E., Deushi, M., Emmons, L. K., Forster, P. M., Horowitz, L. W., Johnson, B., Keeble, J., Lamarque, J.-F., Michou, M., Mills, M. J., Mulcahy, J. P., Myhre, G., Nabat, P., Naik, V., Oshima, N., Schulz, M., Smith, C. J., Takemura, T., Tilmes, S., Wu, T., Zeng, G., and Zhang, J.: Effective radiative forcing from emissions of reactive gases and aerosols – a multi-model comparison, Atmos. Chem. Phys., 21, 853–874, https://doi.org/10.5194/acp-21-853-2021, 2021.

Tromp. T. K., Shia, R.-L., Allen, M., Eiler, J. and Yung, Y. L., Potential environmental impact of hydrogen on the stratosphere, Science, 300, 1740-1742, 2003.

Twomey, S.: The nuclei of natural cloud formation part II: The supersaturation in natural clouds and the variation of cloud droplet concentration, Geofisica Pura e Applicata, 43, 243–249, https://doi.org/10.1007/BF01993560, 1959.

Xiao, X., Prinn, R.G., Simmonds, P.G., Steele, L.P., Novelli, P.C., Huang, J., Langenfelds, R.L., O'Doherty, S., Krummel, P.B., Fraser, P.J. and Porter, L.W. Optimal estimation of the soil uptake rate of molecular hydrogen from the Advanced Global Atmospheric Gases Experiment and other measurements, Journal of Geophysical Research: Atmospheres, 112(D7), 2007.

Yang, H., Waugh, D. W., Orbe, C., Patra, P. K., Jöckel, P., Lamarque, J.-F., Tilmes, S., Kinnison, D., Elkins, J. W., and Dlugokencky, E. J.: Evaluating Simulations of Interhemispheric Transport: Interhemispheric Exchange Time Versus SF6 Age, Geophys. Res. Lett., 46, 1113–1120, https://doi.org/10.1029/2018GL080960, 2019.

Yashiro, H., Sudo, K., Yonemura, S., and Takigawa, M.: The impact of soil uptake on the global distribution of molecular hydrogen: chemical transport model simulation, Atmos. Chem. Phys., 11, 6701–6719, doi:10.5194/acp-11-6701-2011, 2011.

Warwick, N. J., Bekki, S., Nisbet, E. G., and Pyle, J. A.: Impact of a hydrogen economy on the stratosphere and troposphere studied in a 2-D model, Geophys. Res. Lett., 31(5), L05107, doi:10.1029/2003GL019224, 2004.

Zheng, B., Chevallier, F., Yin, Y., Ciais, P., Fortems-Cheiney, A., Deeter, M. N., Parker, R., Wang, Y., Worden, H. and Zhao, Y., Global atmospheric carbon monoxide budget 2000-2017 inferred from multi-species atmospheric inversions, Earth Syst. Sci. Data, 11, 1411-1436, 2019.

# Annex 1: Determining an Hydrogen GWP from steady-state simulations

## Methodology

Fuglestvedt et al. (2010) describe a method by which steady-state simulations can be employed to derive GWPs from indirect forcings. In their method, they assume that the time-integrated radiative forcing of a pulse emission and a one year step emission are equal. The time evolution of the radiative forcing during the step emission is described by an approach to steady-state with a time constant according to the lifetime of the species causing the forcing. The peak forcing is assumed to occur directly at the end of a one year step emission, and the perturbation is subsequently assumed to decay with the same lifetime. For an indirect forcing due to a methane perturbation, the time constant for both the growth and decay phase is assumed to be the methane perturbation lifetime. However, results from transient simulations using our box model and the transient simulation of Derwent et al. (2020) show that the above assumptions do not result in a good approximation of the time evolution of the methane perturbation following a step hydrogen emission. In the transient simulations, the peak in excess methane occurs several years after the end of an $H_2$ step emission rather than immediately at the end of the step emission as is assumed by Fuglestvedt et al. (2010). This difference arises as the Fuglestvedt et al. (2010) equations do not consider the lifetime of the step emission species and are therefore only valid when the lifetime of the step emission species is negligible in comparison to the lifetime of the radiatively active species resulting in the forcing. This is not the case for hydrogen and methane, with atmospheric lifetimes of ~2 and ~12 years (~12 years being the methane perturbation lifetime) respectively. In addition, the assumption that the decay following the peak forcing is controlled only by the lifetime of the radiatively active species neglects any subsequent perturbations to atmospheric chemistry as a result of $H_2$ remaining in the atmosphere after the end of the step emission. We therefore conclude that although this methodology was successfully adopted to present GWPs for short-lived climate forcers in the IPCC Fifth Assessment Report (IPCC, 2014) and implicitly adopted for Global Temperature Change Potentials in the IPCC Sixth Assessment Report (IPCC, 2021), it is not a good approximation for species with intermediate lifetimes (> 1 year), such as $H_2$.

As part of this study, we derive a more universal version of the equations presented in Fuglestvedt et al. (2010) which account for the atmospheric lifetimes of both the step emission gas and the gas causing the indirect forcing. The time period of the step emission can also be varied. A comparison of the time evolution of the methane perturbation resulting from a change in $H_2$ mixing ratio based on the standard Fuglestvedt et al. (2010) equations and our updated equations is shown in Figure A1. Accounting for the atmospheric lifetime of hydrogen in the updated equations results in a predicted slower rate of increase in methane during the step emission relative to the standard Fuglestvedt et al. (2010) equations, a delayed methane peak and a slower rate of methane decrease subsequent to that peak. This difference occurs as the equations from Fuglestvedt et al. (2010) assume that the step emission species has reached a

new steady-state atmospheric concentration by the end of year 1. This is true for short-lived species such as $NO_x$, but not for species with intermediate lifetimes, such as $H_2$.

**Figure A1: The time evolution of excess methane during and after a one year step hydrogen emission (based on a steady-state $H_2$ excess of +1500 ppb, an $H_2$ lifetime of 1.9 years and a methane perturbation lifetime of 12.6 years) as predicted by the Fuglestvedt et al. (2010) equations (yellow) and our updated equations. For our updated equations, the excess methane is split into contributions from methane generated during the step emission (blue), methane generated from excess hydrogen remaining in the atmosphere after the one year step emission (orange), and the total methane excess (grey).**

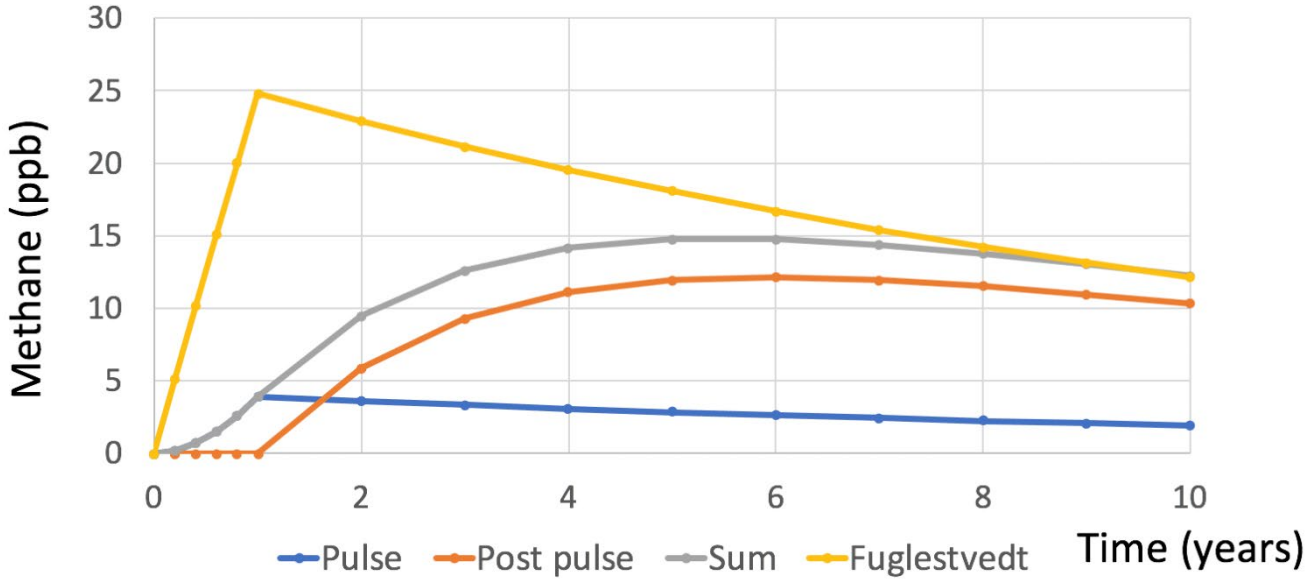


Specifically, our new derivation of the Fuglestvedt et al. (2010) absolute GWP (AGWP) equations accounts for the radiative forcing generated by the chemical perturbation during the step emission (AGWP1), the subsequent decay of the chemical perturbation generated during the step emission (AGWP3), and the chemical perturbation resulting from the step emission species remaining in the atmosphere following the end of the step emission (AGWP2).

$$AGWP1 = R\ a\ \alpha_R\ \alpha_H\ \mathrm{C}\ (tp - \alpha_R \left(1 - \exp\left(\frac{-tp}{\alpha_R}\right)\right) - \left(\frac{\alpha_H}{\alpha_H - \alpha_R}\right) \left(\alpha_H(1 - \exp\left(\frac{-tp}{\alpha_H}\right) - \alpha_M(1 - \exp\left(\frac{-tp}{\alpha_R}\right)\right)\right)) \quad \text{(E1)}$$

$$AGWP2 = \frac{\left(R\ a\ \alpha_H^2\ \alpha_R\ \mathrm{C}\left(1 - \exp\left(\frac{-tp}{\alpha_H}\right)\right)\right)}{\alpha_H - \alpha_R} \left(\alpha_H \left(\exp\left(-\frac{tp}{\alpha_H}\right) - \exp\left(-\frac{H}{\alpha_H}\right)\right) - \alpha_M \left(\exp\left(\frac{-tp}{\alpha_R}\right) - \exp\left(-\frac{H}{\alpha_R}\right)\right)\right) \quad \text{(E2)}$$

`Atmospheric implications of increased hydrogen use

$$AGWP3 = R\ a\ \alpha_R{}^2 \alpha_H\ \mathrm{C}\left(\left(1-\exp\left(-\frac{tp}{\alpha_R}\right)\right)-\left(\frac{\alpha_H}{\alpha_H-\alpha_R}\right)\left(\exp\left(-\frac{tp}{\alpha_H}\right)-\exp\left(-\frac{tp}{\alpha_R}\right)\right)\right)\left(\exp\left(-\frac{tp}{\alpha_R}\right)-\exp\left(-\frac{H}{\alpha_R}\right)\right) \quad \text{(E3)}$$

Where:

AGWP = absolute global warming potential (W $m^{-2}$ $kg^{-1}$ yr)
*R* = radiative forcing scaling factor (W $m^{-2}$ $ppb^{-1}$ or W $m^{-2}$ $DU^{-1}$ for tropospheric $O_3$) (values taken from IPCC AR5, and Myhre et al. 2007)
*a* = production rate of species resulting in the indirect forcing (mixing ratio $yr^{-1}$) per ppb $H_2$ change at steady-state
$\alpha_R$= Lifetime of perturbation to species causing the radiative forcing
$\alpha_H$ = $H_2$ lifetime (combined chemical and deposition lifetime) (yr)
*H* = the time horizon considered, in this study we consider values of 20 and 100 years
*C* = conversion factor for converting $H_2$ mixing ratio (ppb) into $H_2$ mass (kg)
*tp* = length of step emission (yr)

The associated indirect GWPs for each radiative species perturbed by hydrogen are then given by:

$$GWP_{H2} = \frac{AGWP_{H2}}{AGWP_{CO2}} \quad \text{(E4)}$$

where $AGWP_{CO2}(100)$ and $AGWP_{CO2}(20)$ are taken to be 9.17e-14 (± 26%) and 2.49e-14 (± 18%) W $m^{-2}$ $kg^{-1}$ yr (IPCC, 2014) respectively. $AGWP_{H2}$ is taken as the sum of AGWP1-3. The values for $AGWP(100)_{CO2}$ and $AGWP_{CO2}(20)$ change slightly to 8.95e-14 and 2.43e-14 W $m^{-2}$ $kg^{-1}$ yr in IPCC (2021): the impact of this on our $H_2$ GWP calculation, along with other IPCC (2021) updates, is shown in Table 11.

Further details on the perturbation lifetimes for the radiatively active species $\alpha_R$, radiative forcing scaling factors (*R*) and production rates of the radiative forcing species being perturbed by $H_2$ (*a*) are given in the sections for the methane-induced and non-methane induced GWP calculations below. The time length of the step emission is taken to be one year in line with previous studies as this avoids seasonal influences (Fuglestvedt et al., 2010). The conversion factor (*C*) for converting $H_2$ mixing ratio into $H_2$ mass based on UKESM1 data is 3.5e-9 ppb $kg^{-1}$. The representation of the hydrogen lifetime, $\alpha_H$, and its uncertainty is discussed in Section 6.3.

# Calculation of hydrogen GWPs

### GWPs for methane-induced forcings

As shown in Section 4, increases in atmospheric $H_2$ can lead to an indirect radiative forcing from consequent changes in methane, and methane-induced changes in tropospheric ozone and stratospheric water vapour.

$H_2$ GWPs arising from methane and methane-induced forcings are determined using equations E1 to E4. In this case, R is the methane radiative efficiency, defined as 0.000363 (±10%) W $m^{-}$

$^{2}$ (ppb $CH_4$)$^{-1}$ in IPCC, AR5 (this increases to 0.000389 W m$^{-2}$ (ppb $CH_4$)$^{-1}$ in IPCC AR6; the influence of this and other IPCC AR6 updates on our calculations can be seen in Table 11). The methane perturbation lifetime ($\alpha_R$) in UKESM1 is derived to be 12.6 years in this study, which falls within the range given by IPCC, AR5 (12.4 $\pm$ 1.4 years).

Increases in $H_2$ result in a reduction in OH, which decreases the flux through $CH_4$+OH, resulting in an increase in methane mixing ratios. This positive $CH_4$ tendency following an increase in $H_2$ can be considered as an additional methane production rate term (*a*, discussed above) defined as:

$a = CH_4 * k(CH_4+OH) * dOH/dH_2$

where $CH_4$ is the methane lower boundary condition (1835 ppb in UKCA), k($CH_4$+OH) is the global mean airmass-weighted rate constant for the reaction of $CH_4$ with OH and $dOH/dH_2$ is the rate of change of OH with respect to $H_2$. Values for these parameters derived from UKESM1 simulations are presented in Table A1. k($CH_4$+OH) is determined from the gradient of methane lifetime against 1/(global airmass-weighted mean OH), and $dOH/dH_2$ from the gradient of the mass-weighted tropospheric mean OH concentration against $H_2$ surface mixing ratio for the UKESM1 simulations including the feedback on the methane lifetime via an adjusted $CH_4$ lower boundary condition (see Figure 4). It is also possible to derive $dOH/dH_2$ using the gradient of the mass-weighted tropospheric mean OH concentration against $H_2$ surface mixing ratio from the UKESM1 simulations where only the $H_2$ LBC is varied (whilst the $CH_4$ LBC is held constant) in combination with the equation below from Stevenson et al. (2013), and the methane feedback factor of 1.49 derived for UKESM1.

$CH_{4\ new} = CH_{4\ base}\ (\tau_{new}/\tau_{base})^{f}$

where f is the methane feedback factor, $CH_{4\ base}$ and $\tau_{base}$ are the lower boundary condition and chemical lifetime for methane in the base scenario, and $CH_{4new}$ and $\tau_{new}$ are the lower boundary condition and chemical lifetime for methane in the perturbed $H_2$ scenarios. The difference between the $dOH/dH_2$ values derived using the two methods above is negligible in terms of the GWP calculation, and our GWP calculation therefore remains independent of box model results.

**Table A1: UKESM1 values for parameters in equations E1 – E3**

| Value in UKESM1 | |
|---|---|
| $CH_4$ LBC | 1835 ppb |
| k($CH_4$+OH) | 2.8e-15 cm$^3$ molecule s$^{-1}$ |
| $dOH/dH_2$ | 3.68e-9 (dimensionless) |
| A | 1.46e-2 ppb($CH_4$) yr$^{-1}$ ppb($H_2$)$^{-1}$ |

Resulting $H_2$ GWP(100)s arising from changes to the direct methane radiative forcing are shown in Table A2 for the range of $H_2$ lifetimes defined in Section 6.3 (a mean of 1.9 years, with lower and upper limits of 1.4 and 2.2 years respectively). $H_2$ GWPs associated with changes to methane-induced tropospheric ozone and methane-induced stratospheric water vapour are determined by scaling the calculated direct methane forcing using scaling factors of 0.5 (± 55%) and 0.15 ± 70% respectively (IPCC, 2014). Equivalent scaling factors from IPCC (2021) are 0.37 and 0.106. The impact on the $H_2$ GWP of using the IPCC (2021) versus IPCC (2014) scaling factors is shown in Table 11.

**Table A2: Methane-induced hydrogen GWP(100)s including uncertainties arising from the hydrogen soil deposition lifetime, methane radiative efficiency, radiative forcing scaling factors for methane-induced tropospheric ozone and methane-induced stratospheric water vapour and the AGWP for $CO_2$. Radiative forcings at steady state are based on changes in methane mixing ratio derived using the box model for the TS2014_2000$H_2$_2171$CH_4$ UKESM1 simulation and the radiative forcing scaling factors described in this section.**

| Radiatively active species impacted by $H_2$ | Radiative forcing at steady-state (mW $m^{-2}$ $ppbH_2^{-1}$) | GWP(100) including uncertainties in soil deposition lifetime | Uncertainty arising from RF scaling factors & $AGWP(100)_{CO2}$ (standard error) | GWP(100) including $H_2$ soil deposition lifetime and RF scaling factor uncertainties |
|---|---|---|---|---|
| Methane | 0.08 | 4.7 (3.5 – 5.5) | ± 28% | 4.7 (2.5 – 7.0) |
| Methane-induced tropospheric ozone | 0.04 | 2.4 (1.7 – 2.7) | ± 62% | 2.4 (0.7 – 4.5) |
| Methane-induced stratospheric water vapour | 0.01 | 0.7 (0.5-0.8) | ± 75% | 0.7 (0.1-1.4) |
| **Total methane-induced** | **0.13 ± 0.02** | **7.8 (5.7 – 9.0)** | **± 32%** | **7.8 (3.3 – 12.9)** |

### GWPs for non-methane induced forcings

Atmospheric hydrogen can also act as a source of both tropospheric ozone and stratospheric water vapour as well as affecting the stratospheric ozone burden through chemical channels not involving methane. Hydrogen is oxidised to water vapour in the stratosphere and $H_2$ can

also perturb tropospheric ozone via changes to $HO_2$ and $NO_2$. These chemical changes need to be considered in combination with the methane-induced changes to determine an overall GWP for hydrogen.

As for the methane induced forcings, equations E1 to E4 are used to determine hydrogen GWPs for the non-methane induced forcings. The values of parameters required for these equations derived from our UKESM1 simulations are shown in Table A3.

For stratospheric water vapour, the e-folding lifetime of the water vapour perturbation following a change in $H_2$, $\alpha_R$, is derived from model spin-up data following a change to the $H_2$ lower boundary condition and is determined to be 8 years in the lower stratosphere. Values for both R and 'a' are determined from the steady-state change in the stratospheric water profile between our UKESM1 base simulation and the simulation where the $H_2$ lower boundary condition is increased from 500 to 2000 ppb. A comparison of the vertical profile of stratospheric water vapour changes resulting from $H_2$ changes in our study with that resulting from methane changes between 1950 and 2000 in Figure 2b of Myhre et al. (2007), shows very similar $H_2O$ changes at all altitudes. We therefore adopt the radiative forcing determined by Myhre et al. (2007) of 0.05 W $m^{-2}$ with an estimated uncertainty of ±20% for stratospheric water vapour changes relative to base in our TS2014_2000$H_2$ UKESM1 scenario. This water vapour forcing is associated with a change of ~500 ppb in stratospheric water vapour at 30 km altitude, giving a value for R of 1e-4 W $m^{-2}$ (ppb $H_2O$)$^{-1}$ when considering changes at 30 km. We assume that the entire stratospheric $H_2O$ profile will scale proportionally with the $H_2$ lower boundary condition (following results from our UKESM1 simulations using $H_2$ LBCs of 750, 1000 and 2000 ppb $H_2$), so the choice of 30 km for determining R is arbitrary. The production rate of water vapour per ppb change in $H_2$, 'a', can then be defined as the change in steady-state $H_2O$ at 30 km (500 ppb) divided by the lifetime of 8 years and the change in $H_2$ mixing ratio of 1500 ppb.

For changes to the global mean tropospheric ozone column, the value for R is 0.042 (0.037 to 0.047) W $m^{-2}$ $DU^{-1}$ and is taken directly from IPCC, AR5. The e-folding lifetime associated with the ozone perturbation is taken to be 0.07 years, calculated as the tropospheric $O_3$ burden divided by the loss in our UKESM1 base simulation. This is shorter than the lifetime used for the short-lived ozone perturbation in Fuglestvedt et al. (2010) of 0.267 years, however our results are insensitive to the difference between these values and small variations around them. The value for 'a' is calculated as the change in the steady-state global mean tropospheric ozone column in our TS2014_2000$H_2$ simulation relative to base (0.59 DU) divided by the lifetime of 0.07 years and the change in $H_2$ mixing ratio of 1500 ppb.

As described in Section 4.1.3, changes in $H_2$ mixing ratio can also influence stratospheric ozone. In our UKESM1 simulations, the change in global mean stratospheric ozone column between our base and TS2014_2000$H_2$_$CH_4$ (increased $H_2$, including the chemical feedback on the methane lifetime) scenarios was negligible at +0.10 DU, relative to a base value of 283.78 DU, and interannual variations of up to several DU. Based on a value for R for stratospheric ozone of 0.0054 W $m^{-2}$ $DU^{-1}$ (Schwarzkopf and Ramaswamy, 1993), and a range of e-folding lifetimes for the stratospheric ozone perturbation of between 1 and 10 years, this results in a GWP(100) of less than 0.03 using equations E1 to E4. We consider this to be

below the uncertainty involved in the calculation and conclude that changes in stratospheric ozone do not significantly contribute to the hydrogen GWP.

**Table A3: UKESM1 values for parameters in equations E1 – E3**

| | R | A | alphaR |
|---|---|---|---|
| Stratospheric water vapour (at 30 km) | 1e-4 W $m^{-2}$ (ppb $H_2O$)$^{-1}$ | 0.042 ppb $H_2O$ (ppb $H_2$)$^{-1}$ $yr^{-1}$ | 8 years |
| Tropospheric ozone | 0.042 W $m^{-2}$ $DU^{-1}$ | 0.0056 DU (ppb $H_2$)$^{-1}$ $yr^{-1}$ | 0.07 years |

Hydrogen GWP(100)s based on equations E1 to E4, and the parameters in Table A3 are shown in Table A4. As for the hydrogen GWPs based on the methane-induced forcings, we calculate an uncertainty for the GWP(100)s based on uncertainties in the hydrogen soil deposition lifetime and the radiative forcing scaling factors.

**Table A4: Hydrogen GWP(100)s for the indirect radiative forcings arising from non methane-induced changes in stratospheric water vapour and tropospheric ozone. Radiative forcings at steady state are based on the changes in composition calculated in the UKESM1 TS2014_2000$H_2$ simulation and radiative forcing scaling factors described in this section.**

| Radiatively active species (non-methane induced) | Radiative forcing at steady-state (m W $m^{-2}$ ppb$H_2^{-1}$) | GWP(100) including uncertainties in $H_2$ soil deposition lifetime | Uncertainty arising from RF scaling factors and $AGWP_{CO2}$ | GWP(100) including $H_2$ soil deposition lifetime and RF scaling factor uncertainties |
|---|---|---|---|---|
| Stratospheric water vapour | 0.03 ± 20% | 2.3 (1.7 – 2.7) | ± 33% | 2.3 (1.1 – 3.6) |
| Tropospheric ozone | 0.02 ± 12% | 0.8 (0.6 – 1.0) | ± 29% | 0.8 (0.4 – 1.3) |

### Total $H_2$ GWPs

The indirect $H_2$ GWP(100)s calculated above for each radiative species are summed to give a total $H_2$ GWP(100) of 11 ± 5 for a 100 year time horizon, presented in Section 6.4 and Table 11. In Table 11, $H_2$ GWPs are also calculated for a 20 year time horizon and the impact on the GWP of using IPCC (2021) versus IPCC (2014) radiative forcing scaling factors is quantified.

This publication is available from: www.gov.uk/government/publications/atmospheric-implications-of-increased-hydrogen-use

If you need a version of this document in a more accessible format, please email enquiries@beis.gov.uk. Please tell us what format you need. It will help us if you say what assistive technology you use.